M 2014

U.PORTO
FEUP FACULDADE DE ENGENHARIA
UNIVERSIDADE DO PORTO

TESTING NEW THERAPEUTIC AGENTS FOR THE TREATMENT OF AGE-RELATED MACULAR DEGENERATION (AMD)

ANA SOFIA RODRIGUES NETO

MASTER THESIS SUBMITTED FOR THE DEGREE OF
MASTER OF SCIENCE IN BIOMEDICAL ENGINEERING
AT THE FACULTY OF ENGINEERING OF UNIVERSITY OF PORTO

TESTING NEW THERAPEUTIC AGENTS FOR THE TREATMENT OF AGE-RELATED MACULAR DEGENERATION (AMD)

ANA SOFIA RODRIGUES NETO

Supervisor: Ana Paula Pêgo, PhD
INEB – Instituto de Engenharia Biomédica
nBTT - Nanobiomaterials for Targeted Therapies Group

Co-supervisor: Marta Freitas, PhD
INEB – Instituto de Engenharia Biomédica
nBTT - Nanobiomaterials for Targeted Therapies Group

The research described in this thesis was conducted at:
INEB – Instituto de Engenharia Biomédica
nBTT - Nanobiomaterials for Targeted Therapies Group

The research described in this thesis was financed by:
- Fundación General CSIC and Obra Social "La Caixa" (Project BIOAMD)
- Fundação para a Ciência e a Tecnologia and FEDER funds through the Programa Operacional Factores de Competitividade – COMPETE (PEst-C/SAU/LA0002/2013-14)

Acknowledgments

This study is not only the result of an individual effort, but rather a set of efforts that made it possible and without which it would have been much more difficult to get to the end of this step. Therefore, I express my gratitude to all those who were present in moments of distress, anxiety, insecurity, exhaustion and satisfaction.

First of all I would like to thank my supervisors, Dr. Ana Paula Pegô and Dr. Marta Freitas for giving me the opportunity to be part of the Nanobiomaterials for neurosciences team from the nBTT-Nanobiomaterials for Targeted Therapies group and integrate the BIOAMD – biomaterials for modulation of inflammation in Age-related Macular Degeneration project. Thanks for all the guidance, valuable comments and knowledge through the learning process of this master thesis. Their patience and support helped me to overcome many difficult situations and finish this dissertation.

To the Instituto de Cerámica y Vidro (CSIC) from Madrid, Spain and to the Research Center "E. Piaggio" from Pisa, Italy for ,respectively, supplying us different types of Titanium dioxide powders and the microfluidic bioreactor systems, that were essential tools for my work. Thanks for the guidance and knowledge in these fields.

To all my colleagues from Instituto de Engenharia Biomedica (INEB), for always support and help me in my work and for all the fellowship.

To my friends from the “study room” of INEB with whom I shared the most part of the time, specially to Carla Pereira and João Pedro Martins.

To my friends, Margarida Gomes and Pedro Cohen for celebrate with me the important moments and cheer me up on bad moments. Thanks for all the support during these two important years.

To Antony Vieira that despite the distance in this last year, always support me and helped me to stay positive when I was more insecure and exhausted.

To my family, special to my parents and sister, thank you to be unconditional support and always being there when needed.

Abstract

The blood-retinal barrier (BRB), located in the posterior part of the eye, has the role to regulate the microenvironment of retinal visual cells. However, due to some alterations concerning, for instance, the unbalance between the production and degradation of reactive oxygen species (ROS) in the retina, the barrier function can be compromised. As a consequence, some pathological conditions can emerge, like the age-related macular degeneration (AMD), a chronic disease responsible for the loss of central vision due to the gradual deterioration of the macula. Currently there is no way of preventing or curing this form of degeneration.

The BIOAMD - Biomaterials for modulation of inflammation in Age Related Macular Degeneration project proposes a new therapeutic strategy to treat AMD by modulating the ROS unbalance by means of the design of an implantable composite material made from poly(methyl methacrylate) (PMMA) and titanium dioxide (TiO_2). As part of this project, the aim of this thesis was to chemically and, subsequently, biologically (using a barrier system with macrophages) analyze the ROS scavenging capacity of different TiO_2 powders. These included, TiO_2 powders calcined at different temperatures – 200°C, 600°C and 700°C – as well as mixtures of the powders calcined at 200°C and 700°C. The goal was to assess the impact of the different physico-chemical properties of the TiO_2 powders – crystalline network arrangement and grain size – on the ROS scavenging capacity. This was firstly tested under static conditions and then transposes to a dynamic environment, essential to better mimic the *in vivo* conditions, by using a bioreactor system.

Using two distinctive chemical assays based on 2,2-diphenyl-1-picrylhydrazyl (DPPH) or 3-morpholinosyndnomine (SIN-1) it was determined that the 200°C (100 % of anatase phase and with a grain size of 2-30 μm) and 600°C (77 % and 23 % of anatase and rutile phase and with a grain size of 0,5-50 μm) calcined powders, showed the highest percentage of ROS scavenging, which varies from 50% to 70%.

Subsequently the scavenging capacity of the powders of biologically produced ROS was assessed using macrophage cultures. Non-activated or activated macrophages were cultured on transwell membranes. On the bottom of the well plate the TiO_2 powders (200°C or 600°C calcined powders and a commercial powder

containing 6 % and 94 % of anatase and rutile phase and a grain size of 0,5-1µm) were added at two concentrations - 1 mg/ml and 5 mg/ml. The macrophages metabolic activity after 24 hrs and 48 hrs, in all cases, has been kept around 100%. The extra (bottom compartment) and intracellular ROS analysed after 48 hrs were significantly reduced when the macrophages were cultured in the presence of the powders. Noteworthy, no significant differences were verified either between TiO_2 powders or concentrations.

Lastly, the dynamic environment was assessed in a bioreactor system. In a first place was tested its permeability using DPPH and SIN-1 under static, as a control, and dynamic conditions – 150 or 200 µl/min for the bottom chamber and 300 or 400 µl/min for the upper chamber. The results revealed ROS diffusion through the polycarbonate membrane. Nevertheless, it was also possible to observe some interactions between the membrane and the analysed compounds. Afterwards, macrophages were seeded on the top of the membrane and the experiments were performed in static and dynamic conditions – 150 µl/min for the bottom chamber and 300 µl/min for the upper chamber. The results revealed that the presence of flow upon 48 hrs reduces the cell viability. The ROS levels were similar in both chambers. The presence of flow, however, led to an increase in ROS levels in non-activated macrophages indicating a possible activation.

Overall, this work demonstrated that TiO_2 powders, mainly the ones calcined at 200°C and 600°C are good scavengers at both chemical and cellular levels. Furthermore the bioreactor system represents a valuable input for further simulate the BRB and study the TiO_2 based biomaterial in a more reliable eye environment.

Resumo

A barreira hemato-retiniana (BHR), localizada na parte posterior do olho, tem como função regular o microambiente das células visuais da retina. No entanto, devido a algumas alterações como o desequilíbrio entre a produção e degradação de espécies reactivas de oxigénio (ERO) na retina, as funções da barreira podem ficar comprometidas. Como consequência, podem surgir condições patológicas tais como a degeneração macular, relacionada com a idade, (DMRI). Esta é uma doença crónica responsável pela perda de visão central devido à gradual deterioração da macula. Actualmente não existe forma de prevenção ou cura para esta degeneração.

O projecto BIOAMD – biomateriais para a modelação da inflamação na degeneração macular, relacionada com a idade propõe uma nova estratégia terapêutica para o tratamento da DMRI através da modelação do desequilíbrio de ERO usando um material compósito constituído por Poli(metacrilato de metilo) (PMMA) e dióxido de titânio (TiO_2). O objectivo desta tese, como parte integrante do projecto, foi analisar quimicamente e, consequentemente, biologicamente (usando um sistema de barreira constituído por macrófagos) a capacidade de eliminação de ERO por diferentes tipos de pós de TiO_2 calcinados a diversas temperaturas – 200°C, 600°C e 700°C – e também misturas de pós calcinados a 200°C e 700°C. O objectivo foi avaliar o impacto das diferentes propriedades físico-químicas dos pós de TiO2 - arranjo rede cristalina e o tamanho dos grãos - na capacidade de eliminação de ERO. Em primeiro lugar, isto foi testado em condições estáticas e, em seguida, transposto para um ambiente dinâmico, essencial melhor mimetizar as condições *in vivo*, utilizando um sistema de bioreactor.

Usando dois ensaios químicos distintos com base em 2,2-difenil-1-picrilhidrazilo (DPPH) ou 3-morpholinosyndnomine (SIN-1), concluiu-se que os pós calcinados a 200°C (100% de fase de anatase e com um tamanho de grão de 2-30 µm) e 600°C (77% e 23% de fase de anatase e rutilo e com um tamanho de grão de 0,5-50 µm) mostram a maior percentagem de eliminação de ROS, que varia entre 50% a 70%.

Subsequentemente, a capacidade de eliminação de ERO producidos biologicamente pelos pós foi avaliada utilizando culturas de macrófagos. Macrófagos não ativados ou ativados foram cultivadas em membranas transwell. No fundo dos

poços foram colocados os pós de TiO_2 (200°C ou 600°C e pós calcinados um pó comercial contendo 6% e 94% de anatase e rutilo de fase e um tamanho de grão de 0,5-1µm) foram adicionados a dois - concentrações de 1 mg/ml e 5 mg/ml. Em todos os casos, a actividade metabólica dos macrófagos após 24 horas e 48 horas foi mantida a cerca de 100%. Os ERO extracelulares (compartimento inferior) e intracelulares, analisadas após 48 horas, foram significativamente reduzidos quando os macrófagos foram cultivados na presença dos pós. Não foram verificadas diferenças significativas, quer entre os pós de TiO2 ou concentrações.

Por fim, as condições dinâmico foram avaliadas num sistema de bioreactor. Em primeiro lugar foi testado usando a sua permeabilidade, usando de DPPH e SIN-1, em condições estáticas, como um controlo, e as condições dinâmicas - 150 ou 200 µl/min para a câmara inferior e 300 ou 400 µl/min para a câmara superior. Os resultados revelaram um perfil de difusão ROS através da membrana de policarbonato. No entanto, foi também possível observar algumas interacções entre a membrana e os compostos analisados. Em seguida, os macrófagos foram semeados no topo da membrana e as experiências foram realizadas em condições estáticas e dinâmicas - 150 µl/min para a câmara inferior e 300 µl/min para a câmara superior. Os resultados revelaram que a presença de fluxo após 48 horas reduz a viabilidade das células. Os níveis de ERO foram semelhantes em ambas as câmaras. No entanto, a presença de fluxo levou a um aumento nos níveis de ERO nos macrófagos não activados indicando uma possível activação.

Em geral, este trabalho demonstrou que os pós de TiO_2, principalmente os calcinados a 200°C e 600°C, são bons eliminadores de ERO (ERO artificial ou ERO produzidos biologicamente). Além disso, o sistema de bioreactor representa um valioso contributo para simular a BHR e mais tarde estudar os biomateriais à base de TiO2 num sistema que mimetiza mais de perto o ambiente olho.

List of Contents

List of figures

List of Tables

List of abbreviation

aCSF – artificial cerebrospinal fluid

AGEs – Glycosylation end products

AMD – Age-related macular degeneration

BAB – Blood-aqueous barrier

BBB – Blood-brain barrier

BRB – Blood-retinal barrier

CM – Conditioned medium

DCF – 2', 7'-dichlorofluorescein

$DCFDAH_2$ – 2', 7'-dichlorofluorescin diacetate H_2

DPPH – 2,2-diphenyl-1-picrylhydrazy

DR – Diabetic retinopathy

ECM – Extracellular matrix

HIF-1α – Hypoxia-inducible factor 1-alpha

HNE – 4-hydroxynonenal

HRPC – Human retinal progenitor cells

HUVEC – Human umbilical vein endothelial cells

iBRB – Inner blood-retinal barrier

IL-18 – Interleukin-18

IL-1β – Interleukin-1 beta

LFC – Laminar flow chamber

LPS – Lipolysaccharide

MCB – Multi-compartmental chamber

MCmB – Multi-compartmental modular bioreactor

MMP-2 – Metalloproteinase-2

NF-κB – Nuclear factor kappa-light-chain-enhancer of activated B cells

NLR – Non-like receptors

oBRB – Outer blood-retinal barrier

PDGF – Platelet-derived growth product

PDMS – Poly(methylsiloxane)

PGE_2 – Prostaglandin E_2

PKC – Protein kinase C

PMA – Phorbol 12-myristate 13-acetate

PMMA – Poly(methyl methacrylate)

PRRs – Pattern recognition receptors

ROS – Reactive oxygen species

RPE – Retinal pigment epithelium

SD – Standard Deviation

SIN-1 – 3-Morpholinosyndnomine

TEER – Trans-epithelial electrical resistance

THP-1 – Human monocytic leukemia cell line

TNF-α – Tumour necrosis factor-α

VEGF – Vascular endothelial growth factors

ZO-1 – Tight junction protein ZO-1

Chapter 1

Introduction

1.1 Blood-ocular barriers

The inner part of the eye is composed by the aqueous, lens and vitreous and must be protected from direct contact with blood vessels in order to maintain normal visual function. The blood-ocular barriers make this separation possible (1,2). In fact, these barriers are responsible for the protection of the internal ocular tissues from variations that occur in the circulation and are important for the regulation of the inner fluid. Furthermore, these barriers assure the maintenance of the eye highly regulated and chemically defined environment as well as a route to eliminate the waste substances from metabolic activity (2).

The blood-aqueous barrier (BAB) and blood-retinal barrier (BRB) are the two main barriers systems. The BAB is located in the anterior part of the eye and is formed by endothelial cells of the iris blood vessels and a non-pigmented cell layer of the ciliary epithelium. This barrier is responsible for the equilibrium of inflow and outflow of aqueous humor and consequently controls the intraocular pressure. The presence of tight junctions is essential for the prevention of non-specific traverse of solutes into the internal ocular milieu (1).

The BRB is located in the posterior part of the eye and can be subdivided into two structures: the inner part (iBRB) mainly composed by tight junctions between endothelial cells of the retinal vessels and the outer part (oBRB) mainly composed for analogous tight junctions in the retinal pigment epithelium (3). Together, the BRB affects the outward movement of metabolic products from the retina into the blood, thereby regulating the microenvironment of retinal visual cells (2). The loss of natural configuration of BRB and, consequently, its normal functions, leds to the emergence of pathologies such as age-related macular degeneration (AMD) or diabetic retinopathy (DR). Therefore, it is becoming more and more important to have a better knowledge of the BRB and the factors that contribute to its alteration and eventual breakdown.

1.2 Blood-retinal barrier

The localization and the main components of the BRB are schematically represented in Figure 1.1.

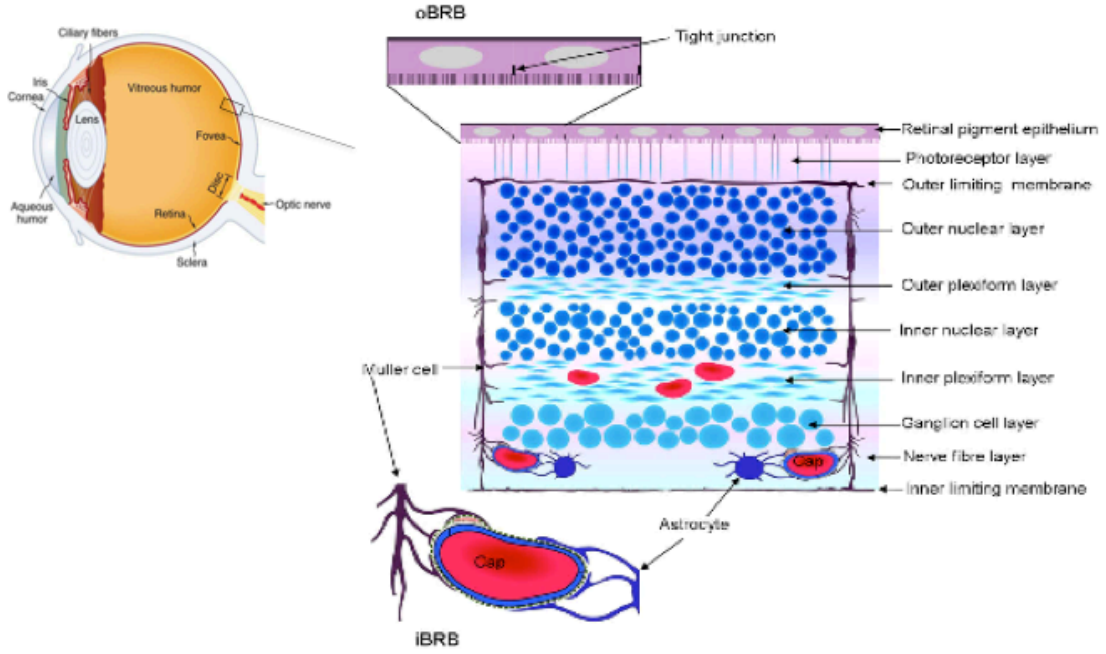

Figure 1.1 – Diagram of an eye cross section and the major cell layers of the retina, emphasizing the inner and outer constitution of the BRB (4).

1.2.1 Inner blood-retinal barrier

Capillary endothelial cells, glial cells (Muller cells and astrocytes) and pericytes constitute the inner blood-retinal barrier (iBRB).

Capillary endothelial cells

Capillary endothelial cells form an endothelium responsible for the establishment of a barrier between the blood and retinal tissue (2). These cells are not fenestrated and have a scarcity of vesicles, responsible for endocytosis or transcytosis (4). Additionally, the narrow intracellular tight junctions of capillary endothelial cells form a network that is only present in vessels from the brain and the retina, although in the retina these tight junctions are slightly more permeable (2).

Glial cells

Muller cells and astrocytes represent the major macroglial cells present in the iBRB (5). These cells, along with pericytes, are associated with the regulation and maintenance of the iBRB. The glial cells are responsible for the uptake of neurotransmitters from nerve terminals but also secrete neuroactive agents like neurotransmitters or neuropeptides and growth factors including vascular endothelial growth factor (VEGF).

Muller cells play an essential role in the regulation of the extracellular space volume, ion and water homeostasis, regulation of the retinal blood flow and in the maintenance of the BRB. Moreover, these cells interact with neurons by providing them throphic substances, removing metabolic waste and supports the synaptic activity by neurotransmitter recycling which involves the supply of its precursors to the neurons (6).

The role of astrocytes in retinal function is less understood. They do not have processes that project to the synaptic layers of the retina and consequently cannot regulate neuronal function similar to the Müller cells (7). Nonetheless, these cells are known to modulate the normal development of retinal vascularization (8). Indeed, astrocytes express VEGF during development (9), which is essential in the angiogenic growth . Therefore, the growth of the inner retinal vasculature is intricately linked with the function of astrocytes.

Pericytes

Pericytes are contractile cells that help to regulate regional blood flow (10). Moreover, pericytes are responsible for the maintenance of capillary structure, inhibition of endothelial cells proliferation and participation in angiogenesis (11)

1.2.2 Outer blood-retinal barrier

The outer blood-retinal barrier (oBRB) is formed by the photoreceptors (rods and cones), the retinal pigment epithelium (RPE) and the Bruch's membrane.

Retinal pigment epithelium

The RPE, located between the photoreceptors and the Bruch's membrane, is formed by a continuous monolayer of cuboidal post-mitotic epithelial cells. The RPE is responsible for the transport of ions, fluid and metabolites via lateral plasma membrane barrier junctions. The transport of ions is crucial for the polarisation/hyperpolarisation of the cell membranes. Moreover, a number of amino acids like taurine, alanine, glutamine and leucine are absorbed across the RPE (12). Additionally, the RPE cells are important in the transport and storage of retinoids, which are fundamental of the visual cycle. The RPE has a phagocytic activity assuring the phagocytosis of the photoreceptors outer segments.

Due to the exposure to visible light and high local oxygen tensions, the RPE emerge as a favourable environment for the production of reactive oxygen species (ROS). These ROS potentiate damage in proteins, DNA and lipids. In this regard, RPE has mechanisms of defence such as enzymatic and non-enzymatic antioxidants that neutralizes ROS before they can cause damage to cellular macromolecules (13,14).

Bruch's membrane

The Bruch's membrane is located between the RPE and the fenestrated choroidal capillaries of the eye. It is divided into three layers: inner collagenous layer, elastin layer and an outer collagenous layer. The two collagenous layers have a similar constitution of collagen type I, II and V, organized in a multilayered grid-like structure. This grid is incorporated in a mass of interacting biomolecules like glycosaminoglycans. The elastin layer is formed by elastin fibers of various shapes and sizes. Collagen type VI, fibronectin and other protein-associated substances also are part of the elastin layer composition. The Bruch's membrane regulates the diffusion of molecules between choroid and RPE. Due to the acellular nature of the membrane, the diffusion is regulated by passive processes. Hydrostatic pressure also regulates the diffusion

through the membrane. Moreover, the Bruch's membrane provides a physical support for RPE cell adhesion, migration and differentiation and a division barrier for choroidal or retinal cell migration (15).

Photoreceptors (rods and cones)

Rods and cones represent the two types of photoreceptors in the retina. They are composed for inner and outer segment. The inner segment contains the nucleus and organelles essentials for the cell metabolism. The outer segment, on the other hand, is the specialized site to detect a photon signal.

Rods are very sensitive to light and respond to a single photon. Due to its high light-sensitivity, rods mediate twilight vision. Comparatively to rods, cones are less sensitive to light and mediate daylight vision. Cones respond to on and off of a light stimulus without significant delays. In this regard, we can follow an object moving quickly with our eyes during daylight (16).

1.3 Alterations of blood-retinal barrier

The BRB has its components and their associated functions well defined. It must ensure the correct passage of fluids into the retina, maintaining the microenvironment of the retina and visual cells (17). Consequently, some alterations in the barrier compromise its functions and may lead to the emergence of pathological conditions.

Aging is associated with some biological changes in the eye mainly in the Bruch's membrane and RPE (18).

With age, the Bruch's membrane alters its molecular composition and physical properties. There is an increase in the collagen cross-linking thereby increasing the strength and density of the collagen network and consequent reduction of the Bruch's membrane elasticity and flexibility. These alterations negatively affect the permeability of the Bruch's membrane. Additionally, from the age of thirty on, the Bruch's membrane starts to calcify and therefore the membrane becomes more brittle and more susceptible to rupture, allowing faster neovascularization. Furthermore, the accumulation of advanced glycosylation end products (AGEs) on structural proteins,

like the collagen in the Bruch's membrane, inhibits protein functions (14). The accumulation of AGEs also influences the production of growth factors, elevating the production of VEGF and platelet-derived growth factor (PDGF) (6). During life there is also a progressive accumulation of lipids in the inner collagen layer forming a lipid wall. The accumulation of lipids damages the capacity of exchange of macromolecules between the choroid and the retina through the Bruch's membrane. Moreover, there is an accumulation of basal deposits and drusens over life. Basal deposits, which are accumulation of waste between RPE and Bruch's membrane, can exist in the form of basal laminar deposits (appear with ageing. It comprises mostly collagen along with laminin, membrane-bound vesicles, and fibronectin) and basal linear deposits (more specific for AMD. It consists primarily of granular and vesicular material with foci of wide-spaced collagen) (18). Drusens are extracellular deposits that accumulate below the RPE in Bruch's membrane. Due to all these alterations, over the years the Bruch's membrane becomes thicker, varying from a thickness of 2 μm in the first decade of life to approximately 4 to 6 μm in the tenth decade of life (19).

Lipofuscin is a variety of coloured lipid-soluble pigments that accumulate in RPE especially during ageing. These granules are not easily degradable and are produced by phagocytosis of shed photoreceptor outer segments (20,21). Additionally, by producing ROS, lipofuscin induce oxidative damage in the RPE and surrounding tissues and inhibit RPE lysosomal enzyme activity (18)

Not only alterations with age but also genetic and/or environment influences play a role in the alterations of BRB. The spontaneous photoreceptor cell loss can also be associated with genetic causes and these can also contribute to the calcification of Bruch's membrane (14). Environmental risks include smoking, exposure to light and tobacco smoke. Smoking leads to an overall increase of oxidative stress since it is associated with the generation of ROS and a decrease of antioxidant capacity. Moreover, smoking is associated with the formation of sub-RPE deposits and accumulation of deposits within the Bruch's membrane (22). The light exposure induces the formation of ROS and may lead to the formation of toxic lipids and protein peroxidation products. The damage caused in the BRB caused by light exposure was found to be correlated with the duration of the exposure, the light wavelength, age,

degree of oxygenation of the retina, genetic factors and endogenous chromophores (23).

The debris accumulated during ageing can cause an attraction of macrophages by the dendritic cells and therefore there an autoimmune response can be triggered and a consequent chronic inflammation.

1.4 In vitro models of the blood-retinal barrier

Since modifications in the BRB are associated with the loss of its functions and a consequent appearance of pathological conditions as described in the previous paragraphs, it was found to be important to study the this barrier in detail, as well as understand the mechanisms behind that trigger these alterations and condition their progress and outcome. Therefore, a number of *in vitro* models of the BRB have been proposed, and found to represent essential tools for the study of the architecture, barrier functions and regulation of the BRB but also to understand the consequences of modifications in the BRB.

These studies have been developed with different cell types, different configuration and in some cases some pathological conditions present in BRB have been successfully simulated. These are discussed in more detail in the following sections.

1.4.1 BRB in vitro models involving two cell types

Darkir and co-workers studied the angiogenic profile of endothelial cells per se in the context of the of the BRB by co-culturing human dermal endothelial and RPE cells (ARPE-19, a spontaneously arising human RPE cell line) in direct and indirect contact (24). The BRB was initially mimicked by plating the RPE cells on the bottom of the plate and the endothelial cells on the top of a 0,4 µm Trans-well insert (Figure 1.2A). As under pathological conditions the rupture of the Bruch´s membrane can occur with the consequent direct contact between endothelial and RPE cells a direct contact system was also proposed (Figure 1.2B), and the pro-angiogenic response evaluated. This study demonstrate that the contact of endothelial and RPE cells

induces the VEGF and matrix metalloproteinase-2 (MMP-2) activity in endothelial cells, thus further enhancing Bruch's membrane degradation and promoting the development of choroidal neovascularization.

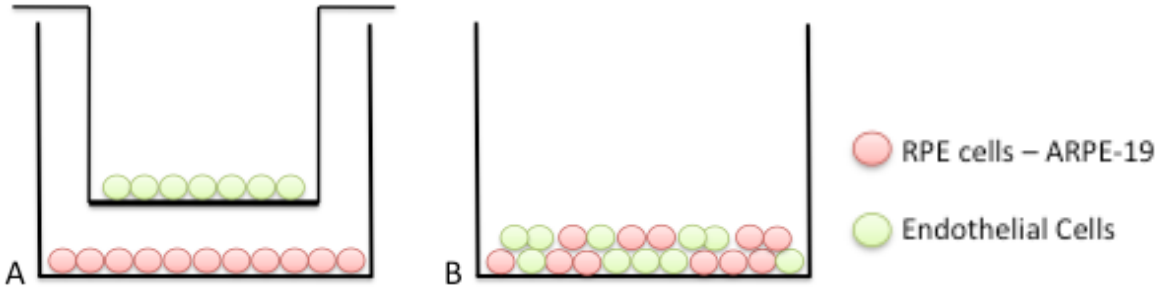

Figure 1.2 – Darkir and co-workers proposed co-culture systems. A – Non-contact RPE and EC co-culture. B – Direct contact co-culture.

Kumar and co-workers used human retinal progenitor cells (HRPC) and human umbilical vein endothelial cells (HUVEC) to simulate the BRB. Two different configurations were established in a 0,4 µm trans-well insert, a non-contact and a contact co-culture system (Figure 1.3). The endothelial cells were seeded on the upper side of the trans-well and the retinal cells on the bottom part, either in the lower chamber (Figure 3A) or in the bottom part of the trans-well (Figure 3B). With these two models the authors intended to evaluate the effect of normoxia and hypoxia. Moreover, monolayer cultures were incubated in normoxia and hypoxia conditions and the biological activity of conditioned medium (CM) was evaluated (Figure 3C) (25).

This study shows that the co-culture under a hypoxia environment resulted in a synergistic increase in the expression of both VEGF and VEGFR-2. Additionally, when HRPC were treated with hypoxia HRPC-CM, the Hypoxia-inducible factor 1-alpha (HIF-1α) and nuclear factor kappa-light-chain-enhancer of activated B cells (NF-κB) normally present in the cytoplasm suffers a translocation to the nucleus.

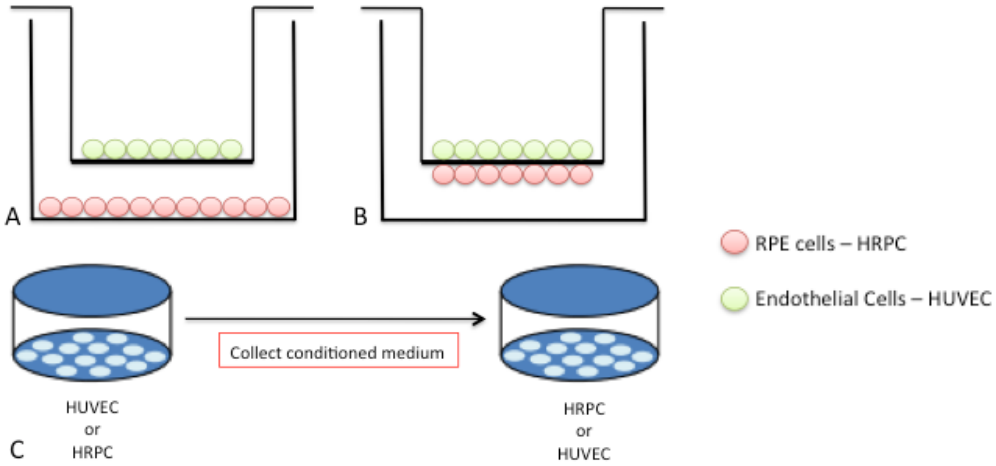

Figure 1.3 – Kumar and co-workers proposed co-culture systems and monocultures. A – Non-contact co-culture. B – Contact co-culture. C – Monocultures with representation of the collection and addition of conditioned medium (Adapted from (25)).

Hamilton and co-workers developed a distinct model of the BRB where they mimicked the Bruch's membrane by using an amniotic membrane and used a minusheet carrier instead of a trans-well membrane. The ARPE-19 cell line and HUVECs were seeded in opposite sides of the same membrane (26). The referred system is present in Figure 1.4. The human amniotic membrane is a thin and elastic tissue that forms the inner layer of amniotic sack. This amniotic membrane bounds to a continuous basement membrane, which is constituted by collagen type IV and laminin, and which interfaces with an avascular collagenous stroma composed of interstitial collagen and elastin (27). In this regard it can be a substitute for the Bruch's membrane due to the similar properties. Moreover, due to its composition, human amniotic membranes are being successfully applied in various fields of medicine, such as ocular surface reconstruction, wound healing, gynaecology and tissue engineering (28).

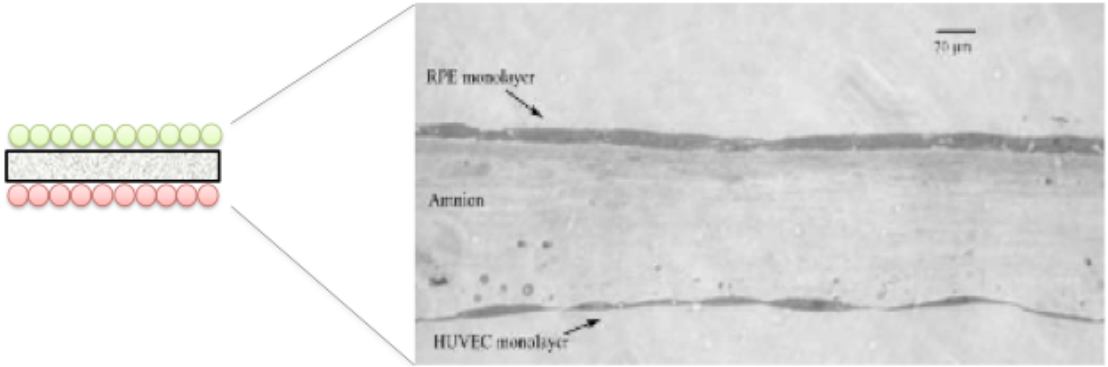

Figure 1.4 – HUVEC and RPE monolayers separated by the amniotic membrane - Transmission electron microscopy (TEM) (Adapted from (26)).

The authors observed the formation of a continuous monolayer of RPE cells and endothelial cells separated by a barrier of biological extracellular matrix. Despite some degree of overlapping, the cells did not form a multilayer. Under co-culture system there was no disturbance in the endothelial adherent junctions warranted by the presence of VE-cadherin at cell-cell contact. Additionally, there was also no alteration in the morphology of RPE cells since the tight junction protein ZO-1 (ZO-1) was still present. Once the system was established in a minusheet carrier, it is possible to introduce flow and having, therefore, a dynamic environment. In this way, the permeability tests were performed under dynamic conditions. The monoculture of ARPE cells with amnion allowed cell confluence. However, despite reduced the leakage of 4-kDa traced, it did not occlude this transfer. On the other hand, the trilayer occlude 95% of the transfer of 4-kDa dextran and 90% of the smaller sodium fluorescein. Moreover, after 3 days in co-culture, a fenestra appears in HUVEC, which did not occur in monoculture, *in vivo* and when co-cultured with other cell type. This alteration in phenotype suggests that there is a RPE-specific cross talk and the plasticity of the cells indicating that the surrounding environment is more determinant than the site of origin.

1.4.2 BRB in vitro models involving three cell types

Wisniewska-Kruk and co-workers studied the contribution of pericytes and astrocytes in the maintenance of BRB (29). In order to achieve their goal, they established five different culture systems using primary cultures of bovine retinal endothelial cells (BREC), bovine retinal pericytes (BRPC) and rat glial cells. Figure 1.5 schematically represents the tested configurations systems.

Glial cells were reported to tighten tight junctions and upregulate and polarize localization of specific blood-brain barrier (BBB) transporters (30), which is a barrier similar to the BRB. However, in the BRB, the contribution of pericytes and astrocytes remains unknown. Additionally, under pathological conditions, Muller cells represent the major producer of VEGF, compromising, therefore, the normal function of the BRB (31). Under these circumstances, the authors proposed different configurations of BRB systems to study the role of pericytes and astrocytes in the mainainence of BRB.

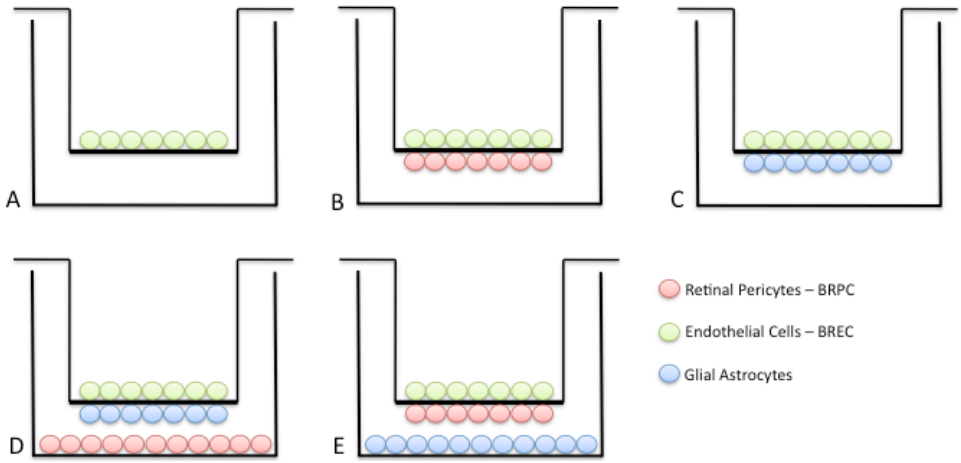

Figure 1.5 – Wisniewska-Kruk and co-workers co-culture systems. A – BRECs monoculture. B – Contact co-culture (BRECs and Glial astrocytes). C – Contact co-culture (BRECs and BRPCs). D, E – Triple co-culture (BRECs, BRPCs and Glial astrocytes).

The tightness of the *in vitro* barriers was evaluated by measuring the trans-epithelial resistance (TEER) values of the barrier. Comparatively to the BREC monoculture, all the co-cultures presented higher TEER values, with the highest value being registered in the triple co-culture with the astrocytes at the bottom side of the insert and pericytes at the bottom of the well (Fig. 5D). Therefore, this indicates that the close proximity between astrocytes and BRECs plays a critical role in the tightening of the BRB. Pericytes themselves do not have a direct influence in tightening the barrier, nonetheless when placed on the bottom of the well and combined with astrocytes there was a substantial increase of the resistance between cells. Additionally to the tightness, it was also evaluated the permeability of the different barriers and the triple co-culture of endothelial cells in contact with astrocytes and pericytes in the bottom of the well significantly reduced VEGF-induced permeability of small molecules.

1.4.3 General overview and discussion of the models

Table 1.1 summarizes the *in vitro* models that were above-mentioned indicating the type and quantity of cells, use of an extracellular matrix (ECM) based scaffold/coating, type of co-culture and in what conditions they were established.

Table 1.1 – Summary of the proposed BRB in vitro models proposed in the open literature.

Cells	Dynamic conditions	ECM	Type of cultures	Reference
Endothelial Cells RPE Cells – ARPE-19	✗	✗	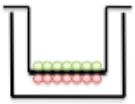	(24)
Endothelial Cells – HUVEC Retinal Cells – HRPC	✗	✗	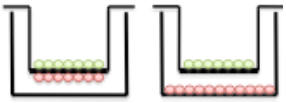	(25)
Endothelial Cells – HUVEC RPE Cells – ARPE-19	✓ ✗	Amniotic Membrane		(26)
Endothelial Cells – BREC Retinal Pericytes – BRPCs Rat Glial Astrocytes	✗	Transwell coating with Collagen type IV	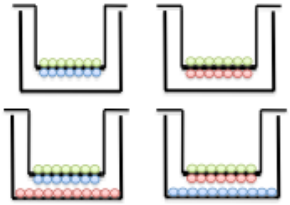	(29)

The proposed BRB *in vitro* models described in the open literature, with exception of the model involving three cell types, were established by using endothelial cells and RPE cells – mimicking the oBRB. Instead of RPE cells, the Wisniewska-Kruk and co-workers established an *in vitro* model by using pericytes and astrocytes aiming at a better knowledge of the role of these cells in the iBRB maintenance. In all cases, the choice of endothelial cell type relied on primary cells: human dermal microvascular endothelial cells, HUVEC and BREC. HUVECs when isolated continue to express signalling molecules that respond to inflammatory mediators, hypoxia and angiogenic growth factors (26). Moreover, this cell type plays an important role as a model system in the study of the regulation of endothelial cell function and the role of the endothelium in the response of the blood vessel wall to stretch and shear stress (32). BRECs can be robustly sub-cultured and are able to maintain a stable phenotype for a long period of time (33). In these studies, the main cell type used to mimic the RPE was the cell line ARPE-19. This cell type is able to polarize and it generates some characteristics of the barrier. They have already been used as a model to study oxidative stress, retinal pathogenesis, signalling pathway and toxicity (34). Kumar and co-workers instead of a cell line used primary HRPCs cells. HRPCs represent only 0,2% of the pigmented cells in the ciliary margin zone. This cell type can differentiate into mature photoreceptors as well. In order to mimic the BRB, Wisniewska-Kruk and co-workers used primary cells, BRPCs and glial astrocyes. Their

choice relies on primary cells because with these cells they can obtain high TEER values and high expression of adherens and tight junctional complexes (29).

In the natural environment of the eye, RPE and choriocapillaries are close to each other, only separated by the Bruch's membrane. In order to mimic as well as possible this environment, the majority of the *in vitro* models of the BRB were established in a trans-well insert with a porosity of 0,4 μm where the cells were seeded on both sides of the membrane, having, therefore, a contact co-culture model. Darkir and co-workers mimicked a simpler model, a non-contact model, where endothelial cells were seeded in the top of the trans-well membrane and RPE cells seeded on the bottom of the well. Kumar and co-workers used both types of co-cultures in order to simulate the BRB. Besides the cell configuration, it is also important to take into consideration the properties of the interface between the cells. In this perspective, Hamilton and co-workers seeded the endothelial and RPE cells on different sides of an amnion membrane, which, as mentioned above, has similar properties to the Bruch's membrane. In a simpler way, Wisniewaska-Kruk and co-workers coated the trans-well membrane with collagen type IV, since it is one of the main components of the ECM.

Despite the permeability tests in the work developed by Hamilton and co-workers that were performed under dynamic conditions, all the models were set up under static conditions. The static conditions however are not able to fully replicate the *in vivo* environment. Indeed, cells are sensitive to their microenvironment, which is rich with 3-D cues from the extracellular matrix, other cells and from mechanical stimuli due to flow, concentration gradients and movements (35). The explored co-culture systems did not offer dynamic chemical or physical stimulus to cells, like concentration gradients, flow, pressure or mechanical stress (36).

1.5 Dynamic models – microfluidic devices

The complexity of the physiological environment involves dynamic interactions between cells and their microenvironment (37). However, the standard *in vitro* cultures, microwell plates or petri dishes, are unable to introduce controlled chemical concentration gradients or physical stimulus like flow and pressure (36,38). With this in mind, various bioreactors systems that allow the culture of cells under dynamic

conditions have been designed. Amongst these are low shear perfusion systems or rotary cell culture reactors where the cells are subject to shear stresses and increased nutrient perfusion, which positively influences cell function. Other bioreactor systems emerge for tissue engineering that provides a high degree of oxygenation through fibres or membranes, allowing adequate oxygen partial pressure with 3-dimentional constructs. Lastly, it has been emerge a generation of microfluidic systems that are becoming more general in laboratories and industries as research tools and are especially suited to performing biological experiments (39). Under microfluidic devices the laminar flow is easily established (40), the cells are able to maintain their own microenvironment and it is possible to study a restrict group of cells by applying a stimulus to that region and observe the response on that cells. The small size of the channels within the microdevices would allow nutrients to difuse to nearby nutrient-poor areas (39). Nonetheless, it is important to mention that these devices also have some drawbacks, such as the difficulty in predicting *in vivo* physiology (36). In this regard, microfluidic system proves to be suitable to mimic the microenvironment present in the BRB. Currently, there are a variety of microfluidic systems and some of them are described below in more detail.

1.5.1 Multi-compartmental chamber

The multi-compartmental chamber (MCB) system was designed with the purpose of mimicking cells of different organs or tissues, which are connected by soluble ligands through blood, lymph, or other fluids in the extracellular matrix (40). Mazzei *et al*. (41) proposed the MCB bioreactor (figure 1.6) to simulate a metabolic system where two different compartmental cell culture chambers were assembled. The first unit mimics the cardiovascular system, in which shear stress and hydrostatic pressure can be applied. The second unit simulates the metabolic system and the chambers with different cell types are cultured in parallels or series.

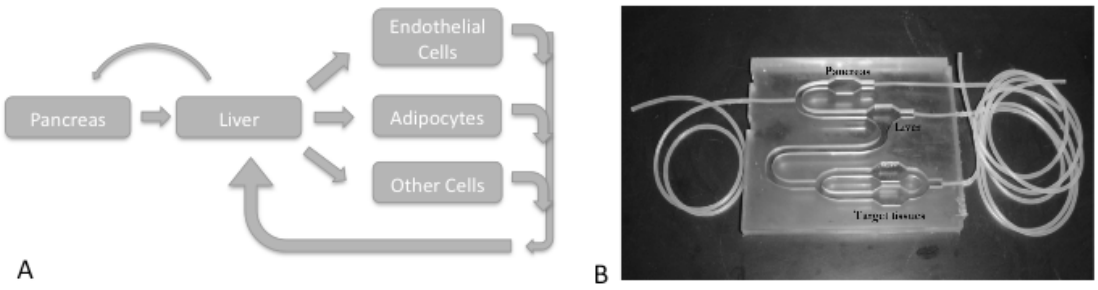

Figure 1.6 – MCB bioreactor. A - MCB chamber topological scheme (Adapted from (41)). B – The MCB bioreactor before assembly, showing the liver, pancreas, and target tissue compartments (40).

1.5.2 Multi-Compartmental modular bioreactor

The multi-compartmental modular bioreactor (MCmB) system is composed of a cell culture chamber that can be linked to other chambers in parallel or in series. In this manner it is possible to mimic different biological systems. The MCmB presents important advantages in comparison to the MCM system where there are a fixed number of compartments. Thus, the MCmB arose as an evolution of MCB system (36,40).

In the first attempt to build this model, some problems emerged leading to the formation of bubbles in the top of the chamber affecting the flow profile and consequently causing turbulence and unknown values of shear stress. To solve this problem, some alterations were introduces in the bioreactor. Namely, increase of the diameter of the chamber (from 13 mm to 15 mm), use of an outlet tube with a larger diameter (from 1 mm to 2 mm) and the introduction of a slope in the top surface of the upper chamber (36). Figure 1.7 represents this system.

Vinci *et al*. (42) seeded isolated hepatocytes from 12 different liver donors into MCmB connected chambers. The authors submitted primary human hepatocytes to culture medium flow, mimicking the blood flow in the liver. The presence of flow specifically interferes, and up-regulate, with the activity of xenosensors and/or expression of detoxification genes in primary human hepatocytes. Under static conditions, there is a down-regulation of detoxification genes probably due to the absence of medium circulation.

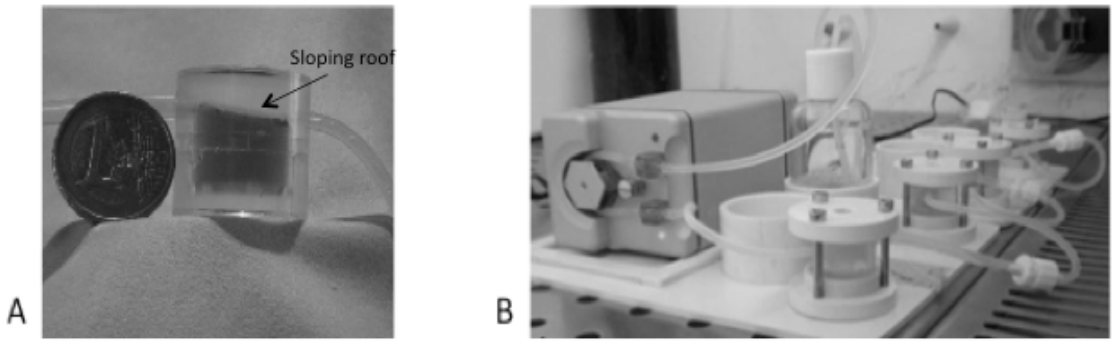

Figure 1.7 – MCmB systems. A – MCmB bioreactor chambers (36). B – Assemble of MCmB bioreactors systems.

1.5.3 Laminar flow chamber

The laminar flow chamber (LFC), represented in figure 1.8 was designed aiming at applying a uniform wall shear stress, which is found in the human vascular system. The purpose of this set-up is also to minimize the internal volume of the cell culture chamber, by reducing the volume of culture medium, and obtain an area similar to the standard ones found in 12 or 24 multi-well plates. Additionally, it allows the placing of the chamber in a regular microscope stage and reduces recirculation regions near the active zone for cell culture (36). This system was used by Vinci *et al*. (37) to seed HUVECs. These authors proved that the application of dynamic conditions on the culture of HUVECs had an impact on their metabolic profile by, for example, increasing the glucose uptake levels.

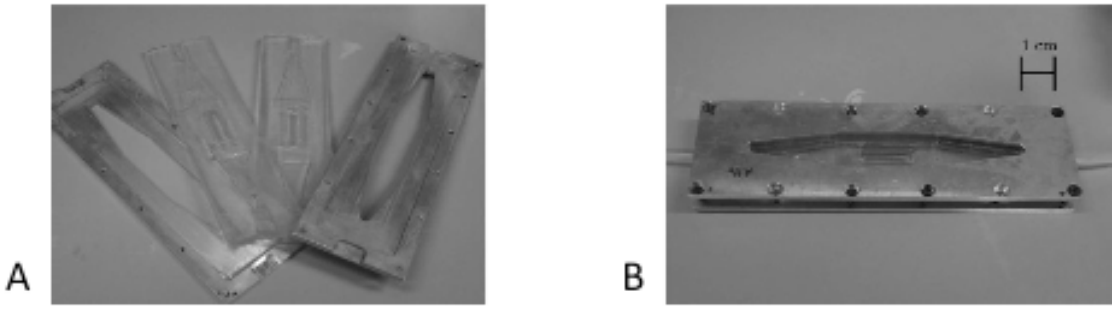

Figure 1.8 – LFC bioreactor. A – The LFC dissembled showing the two halves and the aluminum frame (36). B – The assembled LFC (36).

Vinci and co-workers (35) connected the LCF system with the MCmBs (figure 1.9) in order to investigate the metabolic cross-talk between HUVECs and adipose tissue and the role of hepatocytes in regulating circulating metabolites. While hepatic cells and adipose tissue were cultured in the MCmB 2.0 chambers and consequently subjected to low-shear stress, HUVECs were seeded on the LFC chamber. The

chambers were connected in a closed loop. With this model, it was possible to observe physiological systemic processes, like glucose and lipid metabolism.

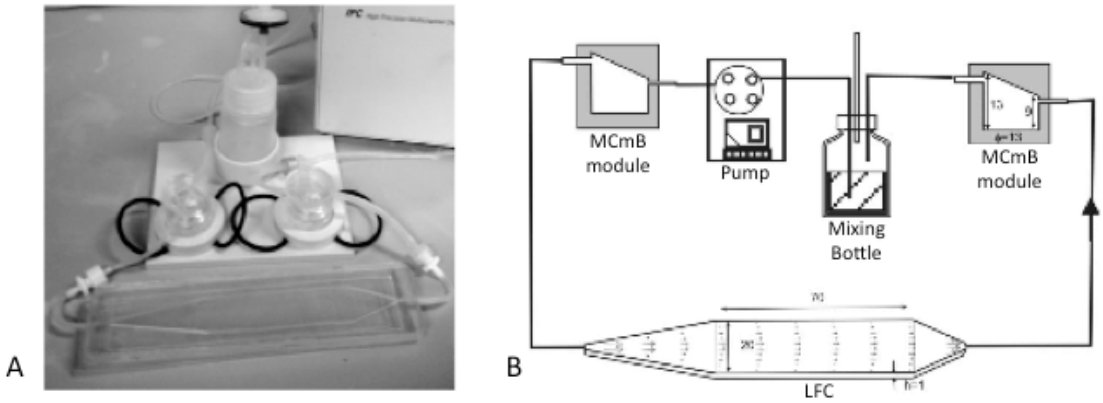

Figure 1.9 – McmB and LFC connected systems. A – Experimental set up (35). B – Connection scheme showing chamber dimensions in mm (35).

1.6 Aim of the thesis

In vitro models of the BRB represent essential tools for the study of eye pathological conditions like AMD. Since dynamic *in vitro* models can incorporate and mimic, not only the biochemical environment, but also the physical stimuli that cells are subjected to in vivo, they provide a better tool to simulate in vitro the environment found in vivo comparatively to static *in vitro* models. Although nowadays it is recognized their importance, there is not a dynamic *in vitro* model for the BRB. Microfluidic devices have emerged as dynamic *in vitro* models and represent an optimal system to mimic the BRB since it is possible to introduce different stimulus and observe their consequences in a small group of cells. Therefore the aim of the thesis is to use a barrier system, which resembles the BRB conditions under a static and dynamic environment, to test new therapeutic agents (in the context of this thesis TiO_2 based biomaterials were assessed) for the treatment of AMD. The dynamic environment will be implemented in a bioreactor previously developed in Pisa University (Italy). Since the retina is highly susceptible to oxidative stress created by the cellular unbalance between production and degradation of ROS, its excess has been associated with the onset and progression of AMD. So the TiO_2 based biomaterials are envisaged as ROS scavengers and, consequently, to be used to halt the progression of this illness.

1.6.1 Age-related macular degeneration (AMD)

AMD is a progressive disease and a leading cause of blindness and visual disability over the age of 50 years in industrial societies. (18,43). This disease develops slowly and asymptomatically in the first years (44). Progressively the patients start to lose central vision making simple tasks like reading a book or driving a true challenge (43). Regarding the progress of AMD, it is possible to divide this pathology into an asymptomatic early stage, and late stage AMD, where vision loss occurs. In the late stage of AMD it can be subdivided into the “dry” and “wet” forms (43,44), characterized either by the absence or presence of choroidal neovascularization, respectively (45). Figure 1.10 shows the different stages of the disease.

Despite some treatments, currently there is no way of curing or preventing this form of degeneration. Nevertheless, with the current knowledge about the disease, different strategies were developed. Since oxidative damage is associated with the progression of the disease, an antioxidant therapy may play a role in reduction the disease progression. With this point of view, some clinical trials prove that the oral administration of an antioxidant combination like vitamic C, vitamic E, beta carotene, zince oxide and cupric oxide had a 25 % relative risk of developing advanced AMD in the other eye (46). Nevertheless, other study demonstrate that oral administration of antioxidants mainly beta carotene increases the risk of lung cancer (47). When the disease is in a later stage is characterized by the choroidal neovascularization, in this regard the treatments are associated with stopping the progression and aid in the regression of choroidal neovascularization. One of the first treatments in this field was the laser photocoagulation, which reveals efficacy in patients with a very well defined choroidal neovascularization (48). However, as a destructive therapy intervention, the patients who underwent this treatment may develop atrophic scars. As an alternative to this treatment, it was develop a photodynamic therapy with verteporfin. This treatment is composed by two phases. The first one concernes the administration of the pharmacologic photo sensitizer intravenously followed by an activation with a laser that has the same wavelength of light absorption as the drug. The results shows that the therapy reduces the risk of vision loss but the improvement of vision is rare (49). Another strategy for the treatment of later AMD concerns to an anti-VEGF therapy.

Several targeting agents have been tested. Pegaptanib (Macugen®) emerge as the first drug approved for that propose, however it this treatment is also accompanied by a loss of vision acuity (50). Following the same strategy, other anti-VEGF drugs were developed and approved like ranibizumab (Lucentis®) (51) and bevacizumab (Avastin®) (52). Despite the evolution in the treatments of AMD, a number of challenges and clinical questions remain.

Early age-related macular degeneration

Early AMD, in a patient's perspective, is hardly symptomatic. Nevertheless, from a clinical point of view, it is characterized by drusens or by hyperpigmentations or small hypopigmentations, without visible choroidal vessels (23,43). Drusens are the formed deposits between the RPE and Bruch's membrane. They can be small, appear flat and be well circumscribed or poorly defined and then can be called as hard or soft, respectively. Hard drusen appear hyaline in cross section, may have a central core that can contain a dentritic cell process extending from a cell with its perikaryon in the choroid proper, and have well-defined edges. They also are more prevalent outside the macula proper and arise most frequently between capillaries in the subjacent choriocapillaries. On the other hand, soft drusens have poorly defined edges and appear more heterogeneous (43).

Late age-related macular degeneration

Late AMD is characterized by two different forms, "dry" and "wet". These two distinct forms can appear in the same patient in different eyes or even in the same eye (23). The pathophysiologies of "dry" and "wet" forms are somehow overlapping, however, they are clinically different since the treatments are different (45).

Physically, "dry" AMD, which is also called geographic atrophy, is characterized by a retinal despigmentation area where choroidal vessels are visible and there is no neovascularization (23,44). The core of dry AMD is the degeneration of areas from the RPE (43,44). Loss of photoreptors and choriocappilaries occurs. Moreover, there is an accumulation of lipofuscin, which can interfere with RPE lysosomal function and

consequently increase autophagy (43). Despite the presence of drusens, they are not sufficient to break the Bruch's membrane.

"Wet" AMD, also referred as neovascular AMD, is characterized by choroidal neovascularization, where new immature blood vessels grow towards the outer retina, leading to leakage of fluid below or within the retina (44,45). The fluid is responsible for the formation of a neovascular membrane (23). The photoreceptor loss is more severe comparatively with dry AMD (46). If left untreated, wet AMD, causes central vision loss (18,23). Patients with subfaveolar choroidal neovascularization develop profound central vision loss regardless of whether the choroidal neovascularization has a classical or occult morphologic feature on angiography (18).

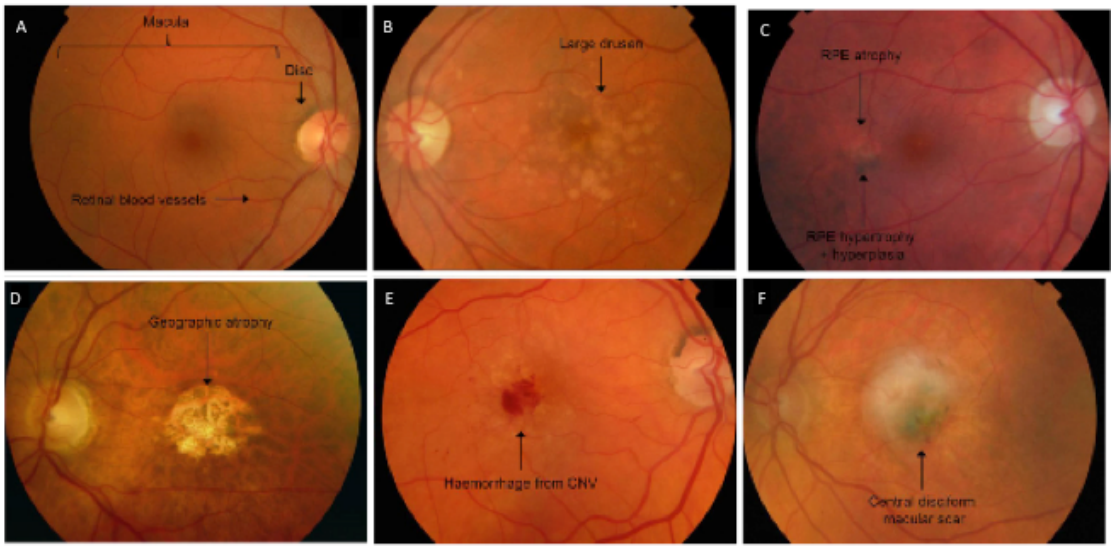

Figure 1.10 – Fundus photographs representing different stages of AMD. A – Normal right eye. B – Early AMD where large drusens can be seen (multiple yellowish clumps). C – Early AMD where it is possible to observe pigment irregularities. An area of hyperpigmentation and hypopigmentation can be seen just temporal to the centre of the macula. D – Late AMD, "dry" AMD, there is an extensive area of sharply demarcated RPE atrophy. E – Late AMD, "wet" AMD, where there is a growth of blood vessels and form a neovascular membrane. It is possible to observe within the image the consequent haemorrhage. F – Late AMD, formation of a scar tissue (47).

1.6.2 Oxidative stress and reactive species of oxygen

As previously stated, the retina is one of the most metabolic active tissues in the body having a high rate of oxygen consumption. Consequently it is more susceptible to oxidative damage caused by the generation of ROS. In order to prevent or diminish the negative effects of oxidative stress, the cells developed different protective mechanisms (48,49). Therefore, a situation of oxidative stress only develops when there is an overproduction and an insufficient elimination of ROS (50). Briefly, ROS are diffusible and highly active molecules. Free radicals, hydrogen peroxide or

singlet oxygen are examples of ROS (50). Cells can produce ROS intracellulary with the purpose of protecting against infection agents and redox-sensitive signalling transduction (51) Nonetheless, once ROS are extracellular released, they can interact with O_2 or other compounds and be involved in oxidative processes (50,51). There are several sources of ROS in the retina. Mitochondria are a major source of endogenous ROS and the existing cross-talk with NADPH oxidase, can represent a "vicious cycle" of ROS production. Mitochondria represent a target for NADPH oxidase-generated ROS and mitochondrial ROS under certain conditions may stimulate NADPH oxidases. Light is essential for vision, however it can lead to the photogeneration of ROS and consequently cause photochemical damage to the retina (48). The exposition to light or in particular to blue light leads to the production of singlet oxygen due to photosensitisation of the macula. The wavelength of the light is intimately related with the amount and type of free radicals. Thus, singlet oxygen can attach to the membranes and other cell components mainly photoreceptor outer segments (50). Furthermore, alcohol consumption and smoking, including tobacco smoke, are exogenous sources of oxidative stress. Alcohol consumption enhances ROS levels, leading to DNA, protein and lipid oxidation. The cigarette smoke is associated with the increase in oxidative stress by the generation of ROS or reduction of antioxidant capacity (48). As mentioned above, there are several mechanisms of defence against oxidative stress in order to create an equilibrium state between ROS production and elimination. Table 1.2 resumes some of those mechanisms:

Table 1.2 – Biologic mechanisms to protect the cells against oxidative stress

Cellular compartmentalization	ROS are separated from cellular components that are susceptible to oxidative damage
Enzymatic antioxidants	Superoxide dismutase, catalase and glutathione peroxidase represent the majority of them
Non-enzymatic antioxidants	Vitamins C, E, and certain carotenoids react directly an in a nonenzymatic way with ROS producing harmless products and terminating the free radical chain reaction
DNA repair	Replacement of DNA portion that was distorted by action of DNA polymerase and closed by the action of a ligase

Some factors like aging, environmental influences and genetic susceptibilities may contribute to create an imbalance in ROS with an increase in the amount of

intracellular oxidizing agents accompanied by a decrease in cell's defence mechanisms (52).

The oxidative stress contributes to RPE dysfunction and lead to the entrapment of abnormal proteins within the Bruch's membrane. Since RPE cells play a principal role in the immune defence of macula, this may lead to autoimmune-mediated inflammation (43,53). Hence, there is a link between oxidative stress and inflammatory system and to observe this link, Kauppinen and co-workers examined if under oxidative stress conditions, the ARPE-19 cell line activates the inflammasome signalling. Briefly, lipid peroxidation end-product 4-hydroxynonenal (HNE), significantly increases the quantity of NLRP-3-specific mRNA in ARPE-19 cells. Innate immune system monitors cellular stress factors through pattern recognition receptors (PRRs) and non-like receptors (NLR), which are the sensing components of inflammasome complex. The inflammasome complexes best known are the NLRP-3 inflammasomes. Moreover, HNE-treated cells produce pro-inflammatory cytokines like Interleukin-1 beta (IL-1β) and Interleukin-18 (IL-18) (53).

1.6.3 Inflammation in AMD

The defence mechanisms in the human body fall into different categories. There is a first line of defence involving a physical barrier, like skin, preventing the entry of pathogens; there is also a second line of defence that involves the innate immune system and includes complement and inflammatory cells (macrophages and recruited leukocytes); in addition there is a third line of defence involving an adaptive immune system that includes clearance of altered pathogens and tissue repair (54).

In the retina, microglia represent the resident inflammatory cells. These cells are similar to the tissue macrophages and the central nervous system microglia. The sub-retinal migration of microglia plays an important role in the elimination of visual by-products and is essential for vision maintenance (55). On the other hand, macrophages can endocytose and remove advanced AGEs, which accumulates in Bruch's membrane throughout life and can increase the secretion of VEGF. Macrophages can also remove the apoptotic cell debris and limit inflammation by inhibiting the production of inflammatory cytokines (56).

An improper activation of immune cells, also play a role in the AMD progression. In fact, in AMD pathology, the microglia accumulates in the subretinal space reflecting a sign of inflammation damage and intensified retinal degeneration (55). On the other hand, macrophages are present in the neovascular membrane and express pro-angiogenic cytokines like VEGF, which indicates that macrophages promote an excessive endothelial cell growth in choroidal neovascularization. In addition to pro-angiogenic proteins, macrophages can also secrete ROS. Furthermore, these cells play an important role in extracellular matrix turnover and express a number of matrix metalloproteases that could lead to Bruch's membrane breakdown (56).

Along with macrophages, dendritic cells are normally present in the retina but reside in the underlying choroid. Nevertheless, in cases of breakdown of the blood–retinal barrier, these cells are recruited from the underlying choroid or from the systemic and accommodate in the retina where they modulate the disease (55). This is noticeable in figure 1.11.

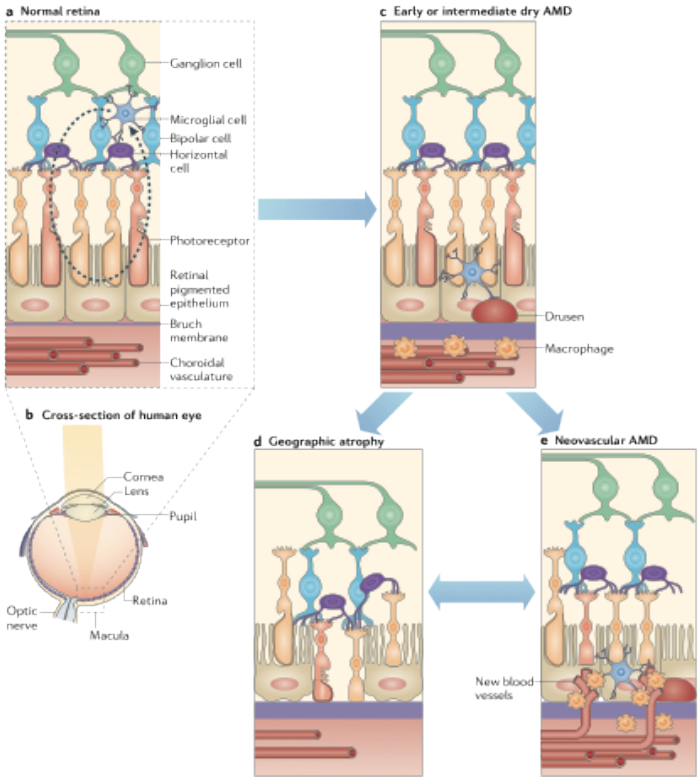

Figure 1.11 – Retinal anatomy in health and disease (55).

Concluding and in accordance with that described, the work plan for my thesis can be divided into three main goals. Firstly, evaluated the ROS scavenging capacity of

different calcined titanium dioxide (TiO_2) powders using artificial ROS. Once chemically evaluated the ROS scavenging capacity of the different powders, the next step was to use ROS produced by macrophages to analyse the ROS scavenging capacity of the most promising TiO_2 powders. Completed this part of the work, the goal was to implement a dynamic system, using a microfluidic device. This system was used to test, chemically, the permeability to the ROS species and further the macrophages were seeded on the membrane and similar tests were performed. This work is part of the BIOAMD – biomaterials for modulation of inflammation in Age-related macular Degeneration project that is in collaboration with the *Instituto de Cerámica y Vidrio del CSIC* from Spain and the University of Pisa in Italy. The main aim is to create an implant biomaterial using TiO_2 and poly(methyl methacrylate) (PMMA) as a substrate. This biomaterial needs to be able to modulate the extracellular microenvironment and connective tissue of the eye in order to prevent and control those inflammatory processes that occur during the progression of the disease. In this regard, the different used TiO_2 powders were produced and provided by the CSIC and the used bioreactor systems were produced and provided by the University of Pisa.

Titanium is a widely used biomaterial. Its biocompatibility is due to the thin surface oxide layer – predominantly TiO_2 – of approximately 4 nm that is spontaneously formed when titanium is exposed to air or oxygen containing solutions (57).

TiO_2 is a semiconductor and when absorbs a photon of light with energy above its valence band gap, an electron from the valence band can be excited to the conduction band yielding an electron-hole pair (e^-/h^+) and consequently is exhibited an potent redox activity. Various species, including hydrogen peroxide (H_2O_2), hydroxyl radical ($HO^\cdot$) and hydroperoxyl radical ($HOO^\cdot$) appear in the irradiated TiO_2 surface (58). On the other hand the presence of titanium dioxide coatings is helpful in the mitigation of the inflammatory response due to the catalytically breaking down of ROS like hydrogen peroxide, superoxide and peroxynitric at physiological pH (59). The neutralization of ROS occurs due to chemical reactions that involve reversible changes in Ti valence and allow to synthesize oxides with enhance anti-inflammatory properties (60).

There are three main crystalline phases of TiO_2, anatase, rutile and brookite, which differ in their physicochemical behaviour. Rutile is the most stable thermodynamically (60). On the other hand, anatase and brookite are metastable and they can be transformed into the rutile phase by heating treatment above 450°C. The transformation from anatase to rutile occurs from 400°C to 1200°C, depending on the grain size, presence of impurities, dopants, precursor material and synthesis method (61). As the calcination temperature increases, the particle size also increases and contrasting the corresponding surface area decreases (62,63). Moreover, a larger surface area is capable to elicit more cytotoxic and phototoxic effects comparatively with smaller surface area (62). The TiO_2 band gaps goes from 3,0 eV in the case of pure rutile to 3,2 eV in the case of pure anatase (64).

In order to further explore the different properties of the powders the collaborating group from CSIC developed different calcined TiO_2 powders and their properties are mentioned in the following tables (Table 1.3 and 1.4).

Table 1.3 – Summary of the physical and crystallochemical characterization of the powders: % anatase, % rutile and % crystallinity.

SAMPLE	% ANATASE	% RUTILE	% CRYSTALLINITY
TiO_2 200°C	100%	0%	50
TiO_2 400°C	100%	0%	75
TiO_2 600°C	77%	23%	100
TiO_2 650°C	13%	87%	---
TiO_2 700°C	3%	97%	---
TiO_2 750°C	2%	98%	---
TiO_2 COMMERCIAL 204757	6%	94%	---

Table 1.4 – Summary of the physical and crystallochemical characterization of the powders: specific surface area, particle size distribution and Band-Gap.

SAMPLE	SURFACE AREA (m^2/g)	PARTICLE SIZE (μM)	BAND-GAP (EV)
TiO_2 200°C	111.2	2-30	3.4
TiO_2 400°C	53.6	2-30	3.32
TiO_2 600°C	10	0.5-50	3.1
TiO_2 650°C	1.9	0.5-70	3.04
TiO_2 700°C	1.2	0.5-70	3.03
TiO_2 750°C	1.4	1-100	3.00
TiO_2 COMMERCIAL 204757	2	0.5-1	3.09

Upon production of the different calcined powders, their ROS scavenging capacity was chemically analysed using artificial ROS (SIN-1 and DPPH methods) Previous results showed that the 600°C calcined powder presented the best percentage of ROS scavenging. This powder is constituted by a mixture of different phases (anatase phase of 77% and rutile phase 23%). Furthermore, we performed mixtures of different ratios of the 200°C calcined powder only at anatase phase, and 700°C, mainly at rutile phase (97 %). The aim was to evaluate if combining powders with different phases, we could obtain a biomaterial exhibiting a higher ROS scavenging capacity.

Our main goal it to verify if TiO_2 is able to degrade the ROS produced by the cells from the BRB mainly RPE and endothelial cells. Nevertheless, it is essential to firstly establish a cellular model. In this way it was used macrophages since it is well known that they produce high levels of ROS upon activation (65,66). Additionally, along with inflammation associated with AMD, the macrophages start to be recruited to the BRB (55).

Chapter 2

Material and Methods

2.1 Materials

The materials used for each assay are described in Appendix A tables. This work is an integral part of the BIOAMD – biomaterials for modulation of inflammation in Age-related macular Degeneration project that is in collaboration with the *Instituto de Cerámica y Vidrio del CSIC* from Spain and the University of Pisa in Italy. In this regard, the different used titanium dioxide powders (TiO_2) were produced and provided by the CSIC and the used bioreactor systems were produced and provided by the University of Pisa.

2.2 Methodology

2.2.1 Chemical Assays

Scavenging of 2,2-diphenyl-1-picrylhydrazyl (DPPH) in the presence of titanium dioxide powders

To assess the ROS scavenging capacity of the titanium dioxide powders a DPPH assay was performed using the protocol described below.

DPPH is a stable free radical in which the capacity to be scavenged can be expressed as a measure of antioxidant activity (67). The purple chromogen radical is reduced, either by direct hydrogen transfer or by indirect electron and proton donation to the corresponding pale yellow hydrazine (figure 2.1). Consequently, there is a decrease of optical density at long wavelengths (515-520 nm) (67,68)

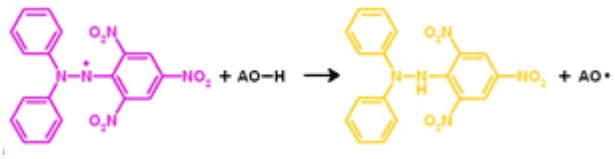

Figure 2.1 – DPPH reduction chemical reaction accompanied by its colour modification.

Firstly it was prepared three replicas of 0,1 mM DPPH solution in the absence of calcined TiO_2 powders. Since there was not ROS scavenging, this represents the maximum DPPH value in solution. In order to analyse the absorbance of the solution, it was added 100 µl from the sample to 400 µl of isopropanol. Subsequently, the absorbance was measured in a spectrophetometer UV-VIS at 517 nm. On the other

hand, it was prepared, as negative control, three replicas with 50 mg of each type of calcined TiO_2 powders (table 2.1) diluted on 500 µl of isopropanol and in the absence of 0,1 mM DPPH solution. In order to analyse the scavenging capacity of TiO_2, three replicas with 50 mg of each type of calcined TiO_2 powder was diluted on 0,1 mM DPPH solution.

Table 2.1 – Different calcined TiO_2 powders and the respective ration of the mixtures

Calcined TiO_2
TiO_2 200°C
TiO_2 700°C
TiO_2 25 % 200°C / 75 % 700°C
TiO_2 50 % 200°C / 50 % 700°C
TiO_2 75 % 200°C / 25 % 700°C

The suspensions were incubated, in the thermomixer and in the dark, for a period of 30 minutes with agitation (1200 rpm) at 21°C. Afterwards, the suspensions were centrifuged (eppendorf 5417R) at 13000 rpm during 3 min and 100 µl of the supernatant were collected and added to 400 µl of isopropanol. The absorbance, proportional to the ROS levels, was measured in a spectrophotometer UV-VIS at 517 nm. The figure below schematically represents the protocol.

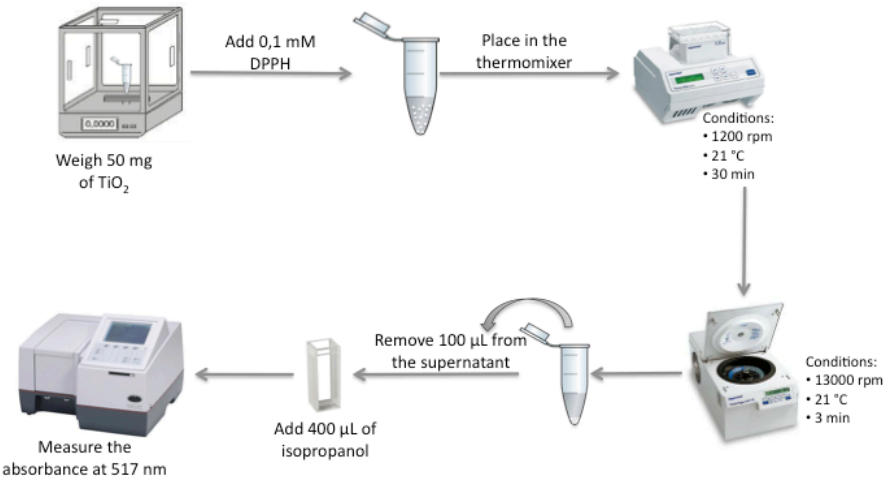

Figure 2.2 – Schematic representation of the DPPH protocol.

Scavenging of 3-Morpholinosyndnomine (SIN-1) in the presence of titanium dioxide powders

SIN-1 (figure 2.3) has been used to generate nitric oxide ($^{\cdot}NO$) and superoxide ($O_2^{\cdot-}$). The reaction between $^{\cdot}NO$ and $O_2^{\cdot-}$ give rise to peroxynitrite ($ONOO^-$), a potent oxidizing agent that plays a causative role in several pathogenic conditions (69).

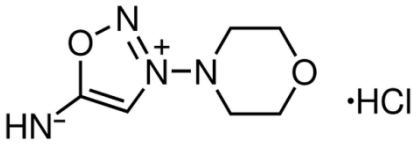

Figure 2.3 – Chemical formula of SIN-1.

SIN-1 was firstly diluted in PBS 1X to a concentration of 10 mM and, afterwards, the final concentration of 25 µM is achieved by diluting the previous solution in aCSF medium. The artificial cerebrospinal fluid (aCSF) medium is constituted by 5 mM KCl, 120 mM NaCl, 1,4 mM $CaCl_2$, 1,2 mM $MgCl_2$, 5 mM D-Glucose and PBS 0,2X.

The procedure used to analyse the scavenging capacity of SIN-1 by different calcined TiO_2 powders was identically to the one used for the DPPH free radical. Firstly, it was prepared three replicas, representing the maximum, of 25 µM SIN-1 solution in the absence of calcined TiO_2 powders. The three replicas of the controls (minimum) was prepared by adding 50 mg of each calcined TiO_2 to 500 µl of aCSF medium in the absence of 25 µM SIN-1 solution. To analyse the scavenging capacity of TiO_2, three replicas three replicas with 50 mg of each type of calcined TiO_2 powder was diluted on 25 µM SIN-1 solution.

The suspensions were incubated, within the thermomixer and in the dark, for a period of 30 minutes with agitation (1200 rpm) at 21°C. Afterwards, the suspensions were centrifuged (eppendorf 5417R) at 13000 rpm during 3 min and 150 µl of the supernatant were collected and 50µl of 250 µM 2', 7'-dichlorofluorescein (DCF) was added. When DCF were in the presence of $ONOO^-$ forms a fluorescent complex and the fluorescence is measured. Briefly, DCF is prepared from its precursor $DCFDAH_2$, which was diluted in PBS 1X to a final concentration of 5 mM. In order to neutralize the solution and therefore obtain DCF, 1600 µL of 0,1 M KOH were added to 400 µL of the

previous solution and the resulting mixture was further incubated at room temperature and in the dark for an additional period of 30 min. After the period of incubation, the solution was diluted with 6 ml of PBS 10X and the DCF reaches to a final concentration of 250 μM. The fluorescence was analyzed in a plate reader (Synergy HT BioTek) using a wavelength of 488 nm of excitation and 517 nm of emission using the Gen5 software.

2.2.2 Cell culture

Human monocytic leukemia cell line culture

In the present study, it was used the human monocytic leukemia cell line (THP-1), purchased from ATCC. THP-1 cells are single, round cells cultured in suspension that resemble primary monocytes and macrophages in morphology and have the typical monocytic markers (70). THP-1 were cultured in RPMI 1640 medium, supplemented with GlutaMax™ a dipeptide (L-alanyl-L-glutamin) substitute for L-Glutamin, know to improve growth efficiency and performance of mammalian cell culture system. The cells were maintained at 37°C and 5% of CO_2.

THP-1 differentiation and activation

The differentiation of THP-1 cell line into macrophages can be induced by treatments with phorbol esters like phorbol 12-myristate 13-acetate (PMA). When exposed to PMA, THP-1 cells adhere to the cell culture plates, acquire a macrophage phenotype with marked morphological changes – flat and amoeboid in shape with well developed Golgi apparatuses, rough endoplasmatic reticula, large number of free ribosomes in the cytoplasm (71). A stock solution of 1 mg/ml of PMA in ethanol was prepared and diluted in the medium to a final concentration of 0,5 μg/ml. The cells were completely differentiated after an incubation period of 48h.

To activate the THP-1 macrophages bacterial lipopolysaccharide (LPS), a major component of gram-negative bacteria and one of the most microbial initiators of inflammation, was used. Cells were seeded in contact with 50 ng/ml LPS for a period of 48 h prior use.

Culture of macrophages in a transwell system in the presence of TiO_2

Macrophages in their basal activity secrete ROS and when activated the secreted ROS levels significantly increase. Therefore, in order to evaluate the macrophage produced ROS scavenging capacity by different TiO_2 powders – commercial and calcined at different temperatures (200°C and 600°C), a non-contact culture transwell system was established (Figure 2.4). TiO_2 powders were weighed (10 mg) and successively suspended in complete culture media in order to achieve different concentrations of powder in suspension (5 mg/ml, 1 mg/ml). These suspensions were added to the bottom of a 12-well plate. The transwells (pore size of 0,4 µm) were added to each well and non-activated or activated macrophages (0,500 x 10^6 cells/well) were seeded on top of the transwell system using complete culture media.

The viability of the cells were analysed after a period of 24hrs or 48hrs of incubation. On the other hand, the presence of ROS in the supernatant and the intrecellular ROS were analysed 48hrs after culture. In both cases were performed cultures of non-activated and activated macrophages.

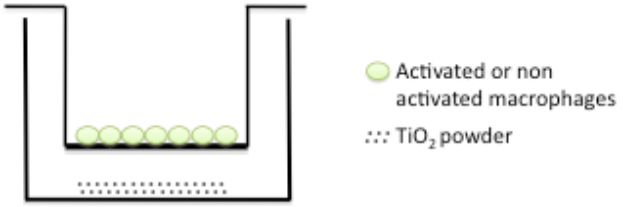

Figure 2.4– Schematic representation of the transwell model. TiO_2 is placed on the lower compartment and the macrophages were seeded on the top of the transwell membrane.

Cell metabolic activity

Cell viability was assessed through the evaluation of the metabolic activity of cells based on the resazurin assay. Briefly, the resazurin assay represents a simple, rapid and sensitive measurement of the assessment of cell viability. The non-fluorescent dye resazurin can be converted in the mitochondria in the strongly fluorescent dye resorufin under the presence of living cells, which are metabolically active (figure 2.5). A resazurin solution was added on both compartments of the transwell to a final concentration of 10 % (v/v) After 4 hrs of incubation, 200 µL of medium were removed from the upper part of the transwell and added into a 96 well

plate and the fluorescence measured in a plate reader (Synergy HT BioTek) using 560 nm excitation / 590 emission filter using the Gen5 software.

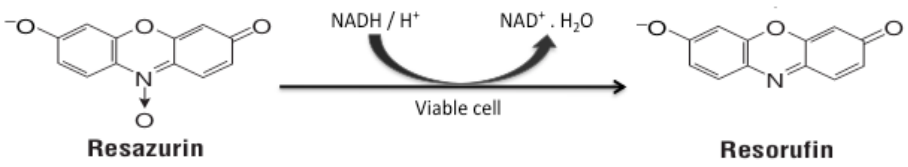

Figure 2.5 – Resazurin chemical reaction.

Evaluation of the presence of ROS in the supernatant

After the set incubation period, 150 µl of supernatant from the bottom and upper compartment of the transwell system was collected and plated in a 96-well plate and 50 µl of 250 µM DCF was added. The fluorescence, proportional to the amount of ROS, was measured in a plate reader (Synergy HT BioTek) using a wavelength of 488 nm of excitation and 517 nm of emission and with Gen5 software. Figure 2.6 schematically represents the used protocol.

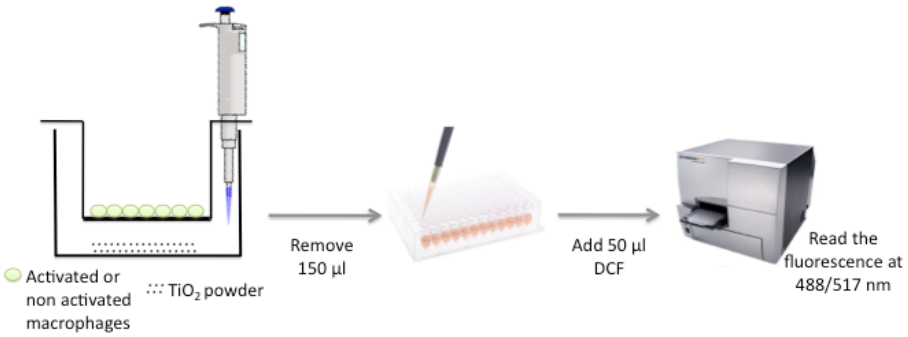

Figure 2.6 – Schematic representation of the evaluation of ROS in the supernatant from basal side.

Evaluation of the presence of ROS inside the cells

After the set incubation period, 10 µl from a solution of 5 mM $DCFDAH_2$ was added into the upper part of the traswell systems. $DCFDAH_2$ is an indicator for ROS in cells. Upon cleavage of the acetate groups by intracellular esterases and oxidation, the compound is converted in the fluorescent compound DCF.

To ensure the incorporation of $DCFDAH_2$ by the cells, they were incubated for 1,5 hrs prior the evaluation with $DCFDAH_2$ in a final concentration of 25 µM. Afterwards the media was removed, cells were trypsinized (350 µl) for a period of 5 to 10 minutes and placed onto a new 12-well plate, and 1 ml of complete media added in

order to inactivate the trypsin. Cells were, subsequently, centrifuged (eppendorf 5417R) at 13000 rpm during 3 minutes and re-suspended in 1 ml of PBS 1X. The presence of intracellular ROS was then analysed by flow cytometry in a FACS Calibur flow cytometer (BD Biosciences) with the Cell Quest software. The obtained results were analyzed using the FlowJo software. Figure 2.7 schematically represents the protocol.

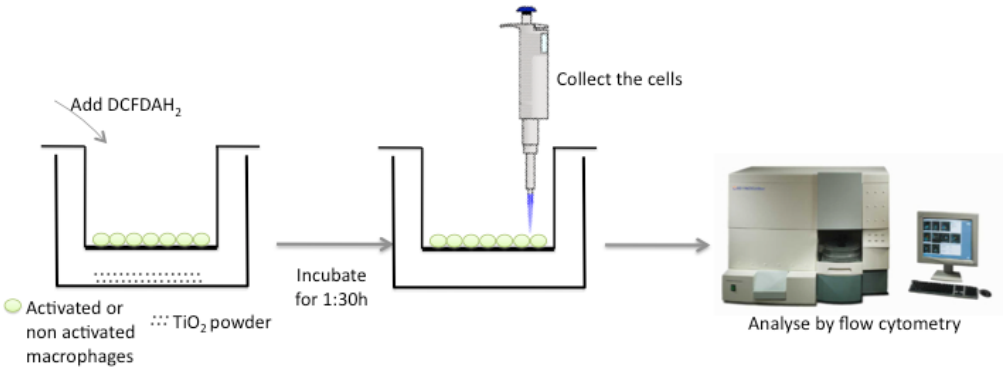

Figure 2.7 – Schematic representation of the evaluation of ROS inside the cells.

2.2.3 Bioreactor

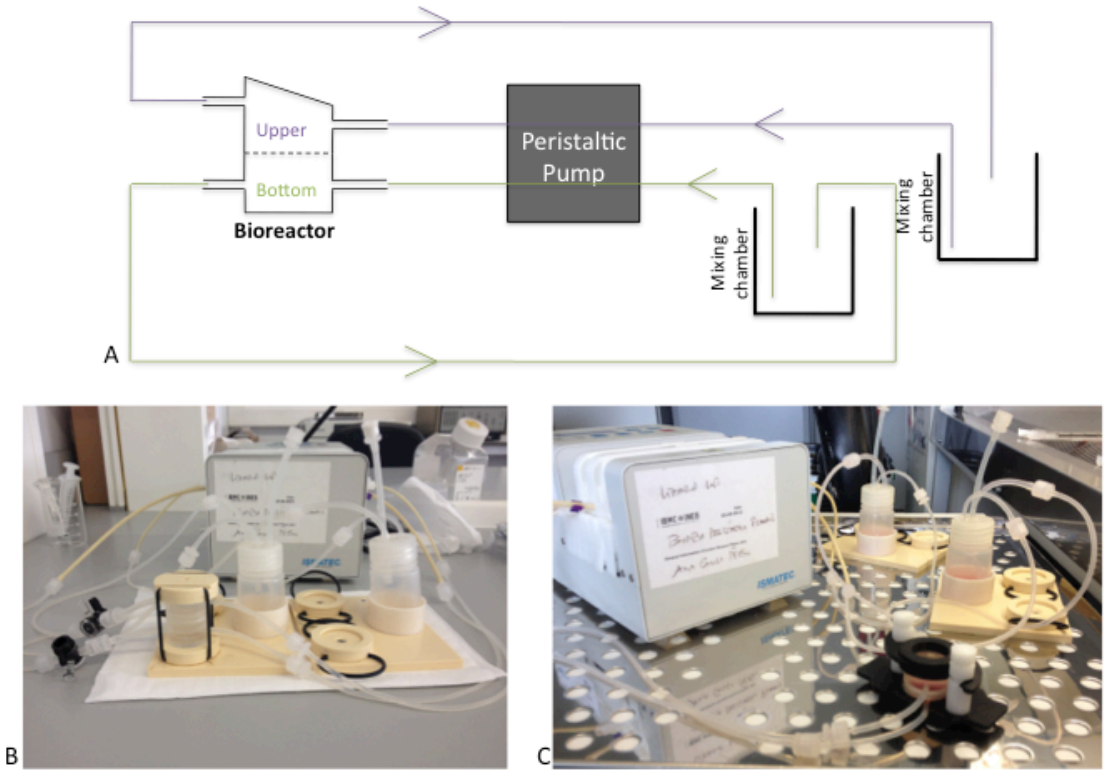

Figure 2.8 – Bioreactor. System A – Schematically representation of the closed-loop bioreactor system. B – bioreactor system. C – new bioreactor system.

The bioreactor, based on poly (methylsiloxane) (PDMS), is mainly composed of an upper, bottom chamber and between them a holder system can be found that supports a polycarbonate membrane. During work we faced some difficulties mainly concerning cell culture. In this regard the components of the bioreactor suffered some modifications and a new system arise. The system is connected to a peristaltic pump (ISMATEC ISM931) that, therefore, induces a flow rate. This flow rate is defined by the setting established in the peristaltic pump and by the diameter of the connecting tube used. An inlet tube goes out from the mixing chamber, which acts as a liquid container, and passes through the peristaltic pump before the connection to the inlet of the chamber. Once the bioreactor chamber is completely filled in, the medium is conducted again to the mixing chamber by an outlet tube. Hence, each chamber is connected in a close loop circuit, as it is observable in figure 2.8.

Upper chamber

The upper chamber (Figure 2.9) has a volume of 1 ml and an inlet and outlet tube with a respectively inner diameter of 1 mm and 2 mm. The presence of an inlet and outlet tube among with the cylindrical shape of the chamber enables the presence of a laminar flow. To assure an efficient bubble removal prior the start of the experiment the inlet and outlet tubes have different inner diameters and the chamber was designed with a slopping roof.

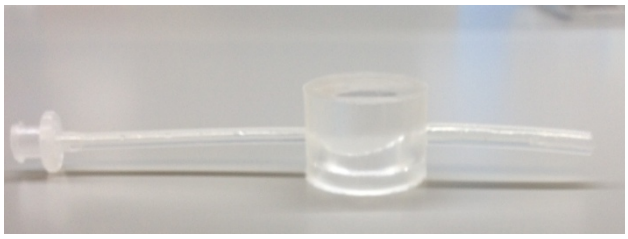

Figure 2.9 – Photograph of the bioreactor upper chamber.

Bottom chamber

The bottom chamber, similar to the upper chamber, has an inlet and outlet tube with 1 mm and 2 mm of inner diameter, respectively, and also a cylindrical shape.

The bottom chamber has a flat silicone base and the coverslips can easily stick to the base hindering the coverslip removal without cause any damage to the cells (figure 2.10A). Moreover, with a partially opaque surface, it is almost impossible to observe the cells in the microscope within the bioreactor system.

As mentioned before, during work a new bioreactor system was developed and the bottom chamber was re-designed in order to eliminate some of its drawbacks. Instead of having just one piece, the chamber is subdivided into three parts: a support for the coverslip (Figure 2.10B), a coverslip (Figure 2.10C) and a ring containing the inlet and outlet tube (Figure 2.10D). Therefore, with these alterations became easier to handle the coverslip and is possible to observe the cells in the microscope within the system. As a consequence of these modifications, the bottom chamber reduces its volume from 1,5 ml to 1 ml.

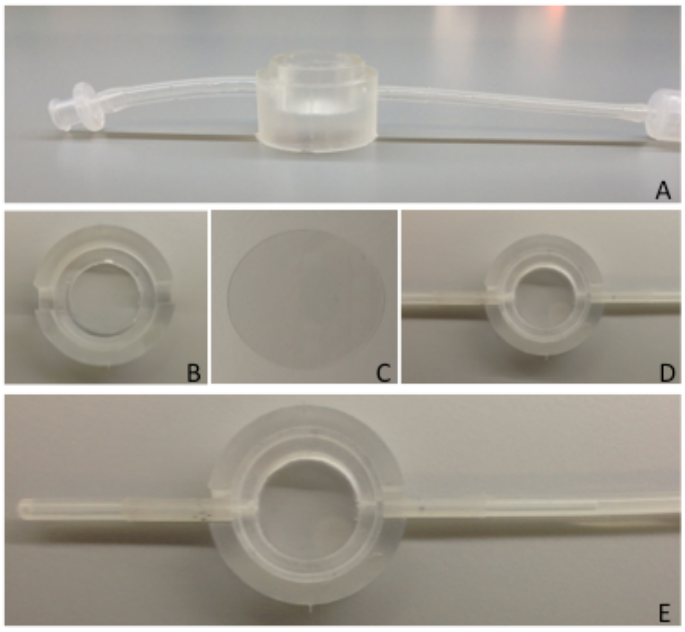

Figure 2.10 – Bottom Chamber. A –Bottom chamber from the first system. B – Support for the coverslip. C – Coverslips. D – ring containing the inlet and outlet tube. E – Connection of the three parts of the bottom chamber, representing the bottom chamber from the second system.

Holder system

The holder system is composed of two cylindrical parts, upper and bottom that connects, due to the male-female joints, to the upper and bottom chambers, respectively. The membrane is inserted between the two parts and once assembled, it can be handled without touching or damaging the membrane. The male joint is part of the upper holder and it is used to press the membrane peripheral region, in order to avoid any misalignment. The central region of the membrane must form a flat, smooth plane in order to allow cell seeding.

In the first bioreactor system these two cylindrical parts were made by PDMS (Figure 2.11A). In the new system, the holder system also underwent some alterations. In order to further reduce the membrane manipulation the material was changed to a stiffer material (Figure 2.11B1 and B2).

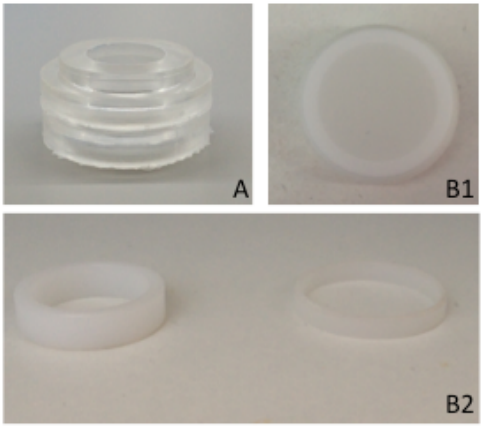

Figure 2.11 – Holder System. A –holder system from the first system. B1 – Holder system of the second system. B2 – The two components of the holder system from the second system.

Clamp system

The clamp system assured the watertightness, since it imposes a suitable pressure to avoid any leakage.

In the first bioreactor system the clamp system (figure 2.12A and B) was constituted of two plastic discs that impress pressure and ensure the water tightness. In order to close the system, there is an O-ring that connects the two discs. A cylindrical slot is needed to insert the bottom chamber and its thickness has to be taken into account in order to avoid the compression of the connecting tubes.

Due to the aforementioned modifications in the bioreactor system and aiming at the visualization of the lower chamber in the microscope, the clamp system of the new bioreactor system experienced some modifications. (Figure 2.12 C and D). To close the system there is a S-clamp system that fits in the slops of the bars present in the support. This support needs also a slot to insert the bottom chamber and also one to fit the inlet and outlet tube due to the reduction of bioreactor size.

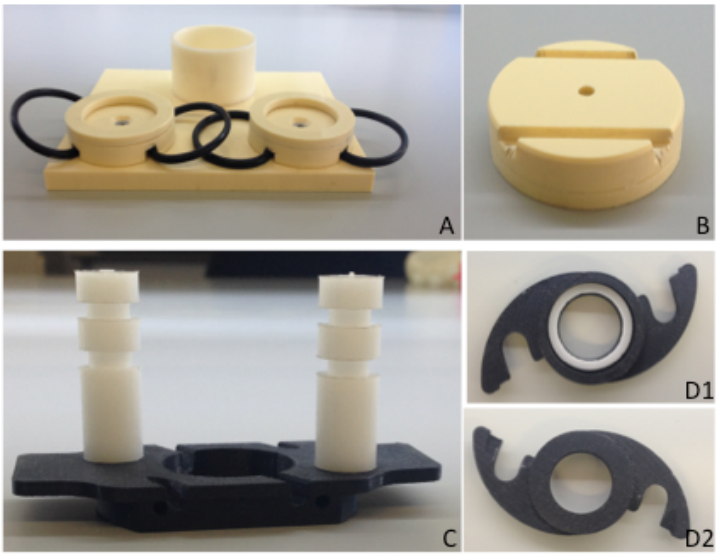

Figure 2.12 – Clamp System. A, B – Clamp System from the first system. C, D – Clamp System from the second system.

Evaluation of the permeability of the system with methylene blue

The permeability of the system was evaluated by using methylene blue. Firstly it was setup a simpler system, under static conditions, where there is no flow and the passage of the compound from the upper to the bottom chamber only occurs due to the gravity force. Subsequently, dynamic conditions were tested at a flow rate of 150 µl/min and 300 µl/min for the bottom and upper chamber, respectively that gave rise to a laminar flow within the chambers. The upper and bottom chamber were, respectively, filled in with 0,25 mg/ml methylene blue and distilled water. Under static conditions the solutions were placed within the chamber with the help of a syringe. The samples were collected with a needle and syringe, which was inserted within the outlet tube of the chamber. Under this strategy of sample removal it was possible to extract the sample from the central part of the bioreactor chamber otherwise it will not be possible to analyse the diffusion of methylene blue. Under dynamic conditions, the compounds were placed within the mixing chamber connected to the upper chamber and with the defined flow rate in the peristaltic pump, the fluid moves from the mixing chamber to the bioreactor chamber. Here, the samples were collected with a connector placed immediately after the outlet tube of each bioreactor chamber. The reading samples were prepared with 25 µl collected from the chamber and 475 µl of

distilled water. Afterwards, the absorbance was measure in a spectrophotometer UV-VIS at 610 nm corresponding to the maximum absorbance of the methylene blue.

Evaluation of the ROS passage through the polycarbonate membrane – DPPH and SIN-1

In order to evaluate the ROS diffusion capacity from the upper to the bottom chamber it was performed assays with DPPH and SIN-1 under static and with SIN-1 under dynamic conditions. It was tested two different conjugation of flow rate, firstly a flow rate equal to the previous one (150 µl/min and 300 µl/min for the bottom and upper chamber, respectively) and then the flow rate was increase to 200 µl/min for the bottom chamber and 400 µl/min for the upper chamber.

Regarding the DPPH assay, the upper chamber was filled in with a 0,1 mM DPPH solution and the bottom chamber with isopropanol. On the other hand, in the SIN-1 assay, the upper chamber was filled in with a 25 µM SIN-1 solution and the bottom chamber with aCSF. The solutions were prepared and the samples measured as mentioned above.

Culture of macrophages in the bioreactor system

The non-activated or activated macrophages were seeded, with a density of 0,500 x 10^6 cells/membrane, on the polycarbonate membrane inside the holder and on a 6 well plate. After 4 hrs the macrophages adhere to the membrane and the holder was sandwiched between the two chambers, which were filled up with complete medium. The apical circuit was filled with 10 ml of complete medium and in the case of activated macrophages, we added LPS in order to keep the activation stimulus. The basal circuit was filled with 10 ml of complete medium. Afterwards, the circuit was closed and a flow rate of 150 µl/min and 300 µl/min for the bottom and upper chamber, respectively, was applied for 48hrs. Additional to the dynamic system, it was established an identical system under static condition as a control.

The macrophages metabolic activity and the ROS passage from the upper to the bottom chamber were analysed after 48hrs of culture.

Cell metabolic activity and evaluation the presence of ROS in the supernatant

After the incubation period and similarly with the chemical assays 150 µl from the supernatant was collected. The presence of ROS was analysed as mentioned above.

In order to evaluate the cell metabolic activity, the chambers were disassembled in a first place and the holder system was transferred to a 12 well plate and it was added completed medium supplemented with 10 % (v/v) of resazurin. After 4 hrs of incubation, it was removed 200 µl from the supernatant and the sample was measured as mentioned above.

2.2.4 Statistical analysis

All statistical analyses were performed with GraphPad Prism® software (Prism 6 for Mac OS X). Data were presented as mean ± standard deviation (SD). Student's t-test was used to compare two sets of measurements. To determin how a response is affected by two factors was used the two-way ANOVA complemented with Tukey's multiple comparisons test. Differences at $P< 0,05$ were considered to be statistically significant.

Chapter 3

Results and discussion

3.1 Chemical Assays

3.1.1 Scavenging of 2,2-diphenyl-1-picrylhydrazyl (DPPH) in the presence of titanium dioxide (TiO_2)

The ROS scavenging capacity of the different TiO_2 powders mixtures are represented in Figure 3.1. The graphic also presents the ROS scavenging capacity of the commercial 204757 and 600°C powders, as controls.

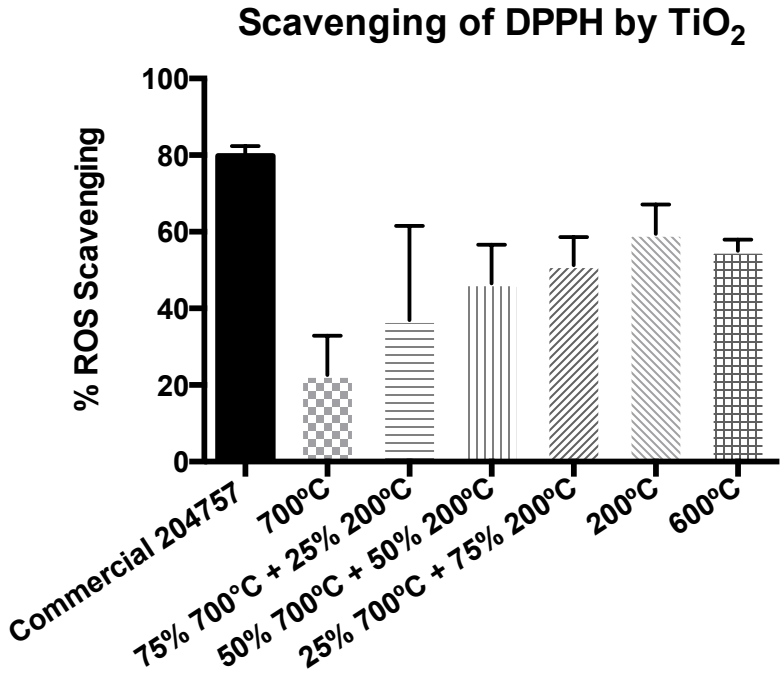

Figure 3.1 – Graphic representing the percentage of scavenging of DPPH by the different TiO_2 powders. Data represents the mean ± standard deviation (S.D), (n=3).

The scavenging capacity of 200°C and 700°C TiO_2 powders were, respectively, 60% and 23%, whereas the scavenging capacity of the mixtures with different ratios of both TiO_2 powders varies from 37% to 51%. Therefore, these results reveal that the combination of different ratios of the 200°C and 700°C calcined powders did not improve the scavenging capacity of DPPH. Also, these results show that the 200°C calcined powder presents a high ROS scavenging capacity.

3.1.2 Scavenging of 3-Morpholinosyndnomine (SIN-1) in the presence of titanium dioxide (TiO_2)

A similar assay was performed with SIN-1. The assay with SIN-1 represents a better correlation with the physiological conditions. This correlation is achieved since DPPH is diluted in isopropanol (non physiological solution) and SIN-1 is diluted in aCSF medium forming a physiological solution. The results are presented in figure 3.2.

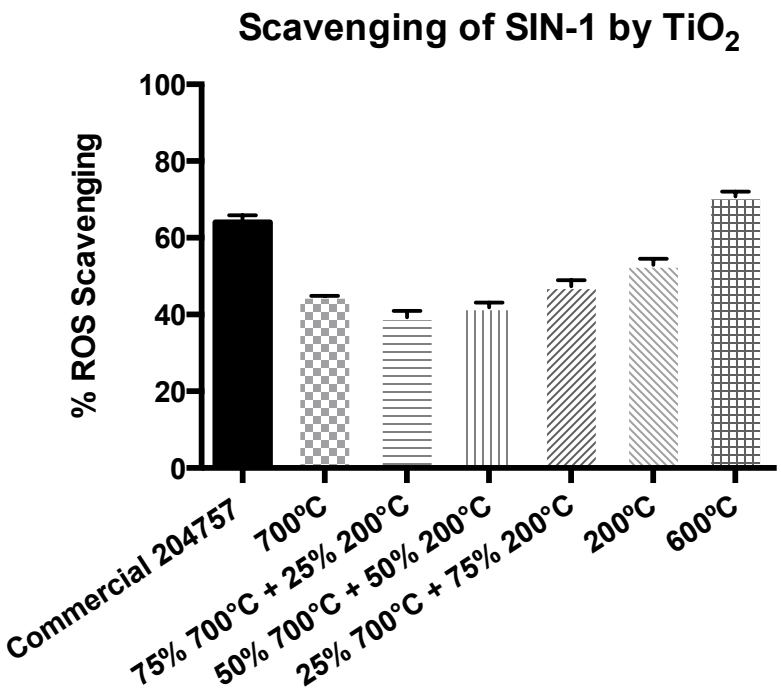

Figure 3.2 – Graphic representing the percentage of scavenging of SIN-1 by the different TiO_2 powders. Data represents the mean ± S.D, (n=2).

As showed in the previous results with DPPH, the results of SIN-1 scavenging by the mixture of different powders also include previous results of the commercial and 600°C powder, as controls. Even with SIN-1, there is a tendency to obtain better scavenging of ROS by the powders individually. Indeed, the scavenging capacity of 200°C and 700°C powders was 52% and 44%, respectively and the scavenging percentage of the different mixtures were in between, varying from 39% to 47%.

All together, these results pointed out that comparatively to the mixtures, the individual powders have a higher scavenging capacity and the 200°C and 600°C appear to be the most promising TiO_2 powders.

3.2 Cell Culture

Once chemically analysed the TiO_2 scavenging capacity and concluded that the 200°C and 600°C powders seems to have the most promising scavenging capacity, the following step is to analyse the TiO_2 scavenging capacity of the ROS produced by macrophages. The used TiO_2 powders are the 200°C and 600°C along with the commercial 204757 as a control. Therefore, the assays with macrophages were performed with these powders.

3.2.1 Human monocytic leukemia cell line expansion

Macrophages can be derived from the THP-1 cell line, which are single, round suspension cells (Figure 3.3). This cell line has some advantages over human primary monocytes-macrophages. Their homogeneous genetic background minimizes the degree of variability in the cell phenotype. Moreover, THP-1 can be stored indefinitely in liquid nitrogen. Following an appropriate procedure, this cell line can be recovered without obvious detrimental effect on monocyte-macrophage features and cell viability (71). Once differentiated and activated, the macrophages produce ROS and the TiO_2 scavenging capacity can be analysed.

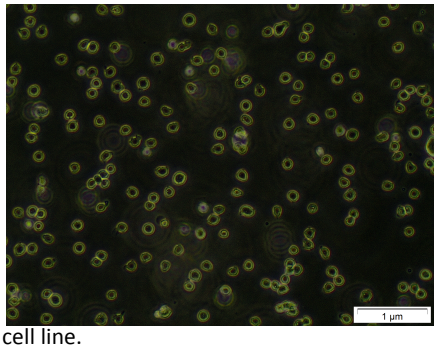

Figure 3.3 – Undifferentiated THP-1 cell line.

3.2.2 THP-1 differentiation and its activation

THP-1 can be differentiated into macrophages by using PMA. Under differentiation, the cells start to adhere to the cell culture flask and acquire a more enlongated morphology that is maintained when macrophages are activated with LPS (Figure 3.4).

PMA-differentiated THP-1 cells enhance the phagocytic activity, release of O_2^-, formation of tumour necrosis factor-α (TNF-α), and prostaglandin E_2 (PGE_2) and expression of the surface antigens CD11b and CD14. Lastly, phorbol esters are known to activate protein kinase C (PKC). Indeed, after differentiation with phorbol esters there is a translocation of PKC isoenzymes -α and -β to cellular membranes suggesting that these isoenzymes might be involved in differentiation process (73).

LPS is a complex glycolipid composed of a hydrophilic polysaccharide moiety and a hydrophobic domain known as lipid A. LPS induces the production of proinflamatory cytokines in macrophages like TNF-α and IL-1, -6, -8, and -12. Moreover, when activated, macrophages also secrete other biological response mediators including free radicals, such as nitric acid (74).

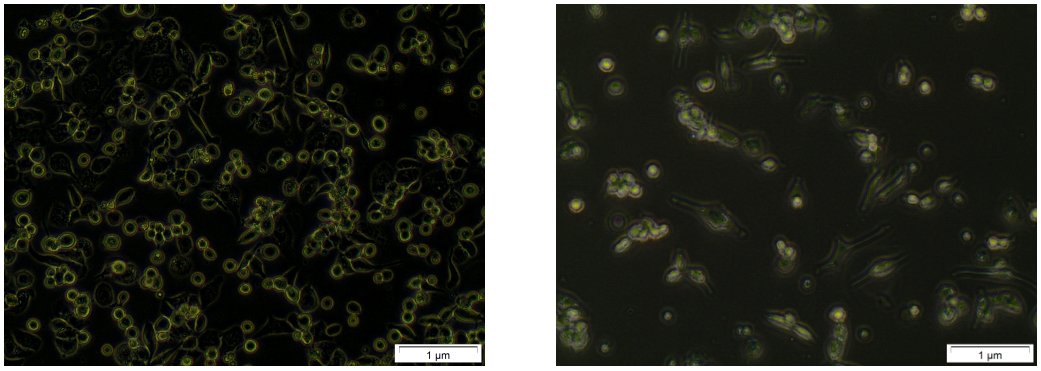

Non-activated Macrophages Activated Macrophages

Figure 3.4 – THP-1 derived macrophages (differentiated with PMA (48 hrs) and subsequently activated with LPS (48 hrs))

As mentioned before, when macrophages are activated and exhibit an inflammatory profile, they produce higher levels of ROS. To confirm this, levels of intracellular ROS before and after macrophage activation were analysed by flow cytometry (Figure 3.5).

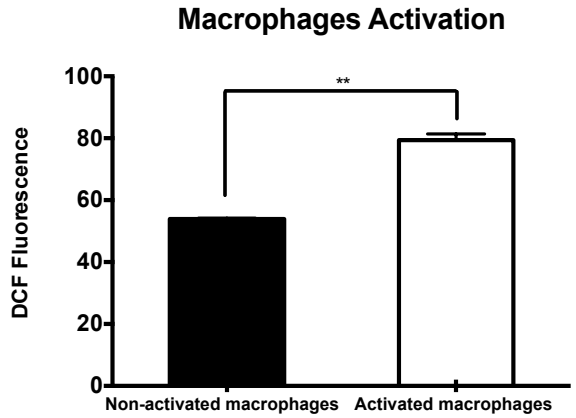

Figure 3.5 – DCF fluorescence, (quantified by flow cytometry after the macrophages were 1,5 hrs in contact with $DCFDAH_2$) proportional to the intracellular ROS. Data represents the mean ± S.D, (n=2), ** p <0,01 within the activated macrophages compared to the non-activated macrophages as determine by t test.

The results show that when activated, macrophages present higher fluorescence, which is proportional to the amount of ROS, comparatively to the non-activated macrophages.

3.2.3 Culture of Macrophages in a transwell system in the presence of TiO_2 powders

In previous assays, it was established a model where the macrophages were in direct contact with the powders. In this work, in order to resemble the BRB, it was establish a transwel system where macrophages were placed in the apical side and different powders at different concentrations in the basal side.

3.2.4 Evaluation of the metabolic activity of macrophages

The non-activated or activated macrophages are placed into the apical side of the transwell system and the TiO_2 powders on the basal side.

In order to investigate whether TiO_2 powders, even not being in direct contact, presented a cytotoxic effect on non-activated or activated macrophages, they were incubated with distinguish types of TiO_2 powders at two different concentration. After 24h or 48h of culture the metabolic activity were assessed by adding resazurin and afterwards the fluorescence was measured (Figure 3.6).

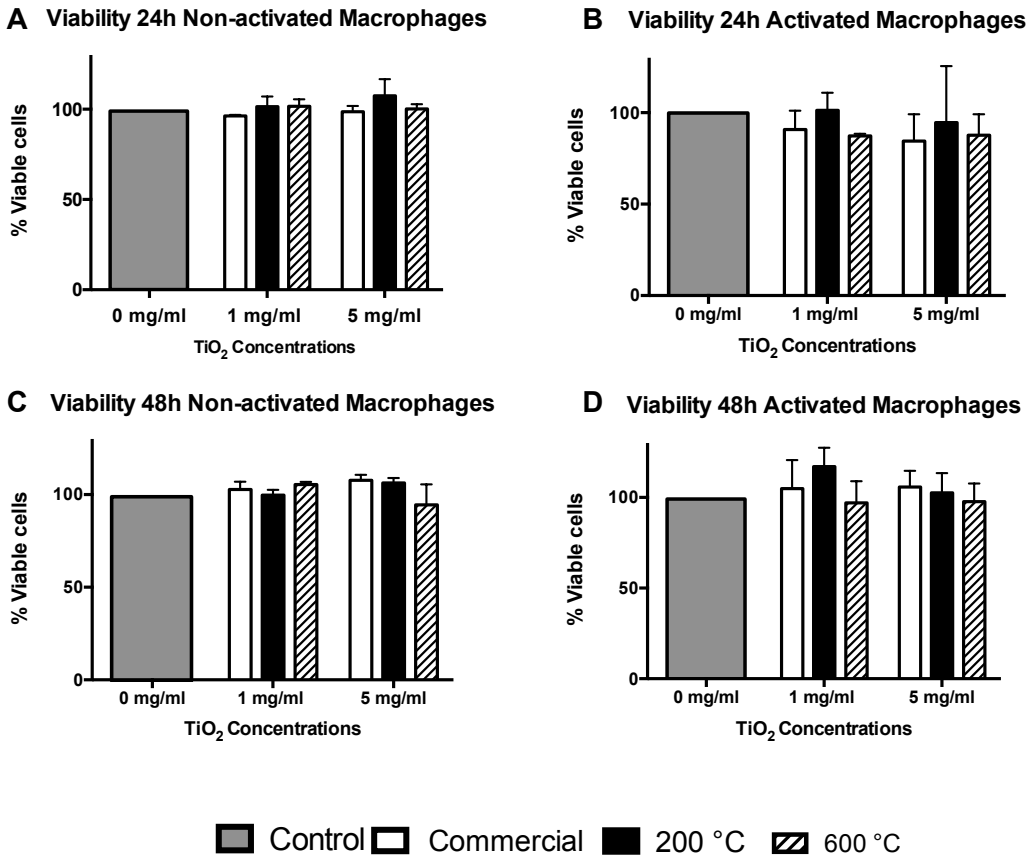

Figure 3.6 – Cell metabolic activity after 24h and 48h of culture. A – Viability after 24h of the non-activated macrophages. A – Viability after 24h of the activated macrophages. C – Viability after 48h of the non-activated macrophages. D – Viability after 48h of the activated macrophages. Data represents the mean ± S.D, (n=2-3),

The metabolic activity of macrophages was not significantly affected either after 24h or 48h in the presence of the different TiO_2 calcined powders.

Our findings showed that macrophages maintained their metabolic activity and are not suffering a direct toxic effect by these TiO_2 powders. Moreover, the increase of TiO_2 concentration did not reduce nor increased the metabolic activity.

3.2.5 Evaluation of the presence of ROS in the supernatant

Since the TiO_2 powders do not affect cell metabolic activity, we proceed to the analysis of the ROS scavenging capacity of the powders. We analysed the ROS released by the cells to the medium, here after referred as extracellular ROS and the ROS the is retained inside the cells, here after referred as intracellular ROS.

Once it was shown that the metabolic activity is not affected in the presence of the TiO_2 powders at different concentrations and taking into account previous results

where the macrophages were in direct contact with the powders, it was decided to pursue the analysis after 48h under the presence of powders. In this regard, Figure 3.7 shows the extracellular ROS results.

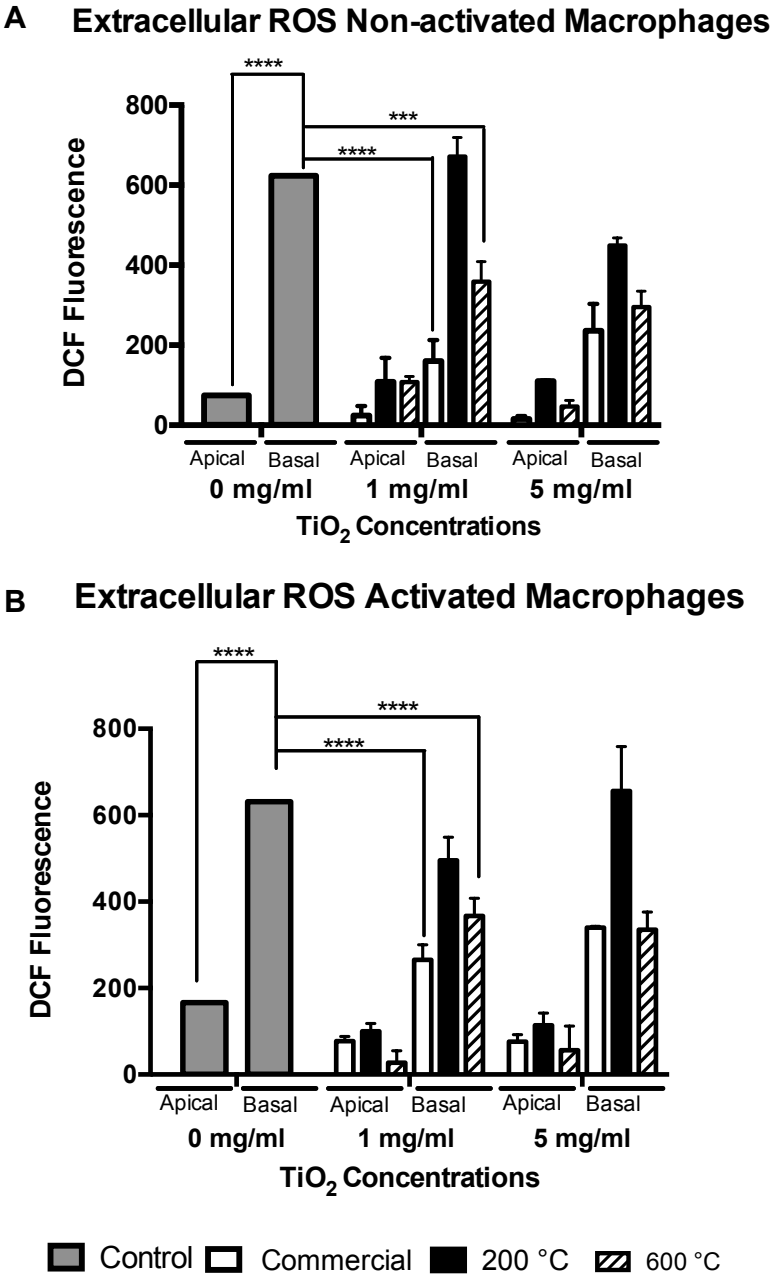

Figure 3.7 – DCF fluorescence, proportional to the extracellular ROS after 48h of culture in the presence of powders. A – Extracellular ROS of the non-activated macrophages. B – Extracellular ROS of the activated macrophages. Data represents the mean ± S.D, (n=2), *** p <0,001, **** p <0,0001 within supernatant from the basal side compared with the supernatant from the apical side in the absence of powders and within supernatant from the basal side in the presence of 1 mg/ml of the TiO_2 powders compared to the supernatant from the basal side in the absence of powders. These statistic differences were determined by 2way ANOVA, using Tukey's multiple comparison test.

First of all, it is important to mention that in both, non-activated or activated macrophages, the ROS levels normally follow the same tendency but yet the initial

levels of supernatant ROS in the activated macrophages were higher than in the non-activated macrophages.

After 48h of culture, when there are no TiO_2 powders in the system, there is a residual ROS level on the apical side that is significantly lower comparatively to the ROS levels on basal side. This result suggests that upon ROS production by macrophages in the apical side they move into the basal side.

Furthermore, when 1 mg/ml of TiO_2 powder is introduced into the system the ROS levels are significantly reduced, with the exception of 200°C powder, where it was not observed any differences relatively to the ROS levels in the absence of the TiO_2 powder. The same profile is observed when the concentration of the different types of TiO_2 powders is increased. Therefore, these results suggest that the increase in TiO_2 concentration do not improve the ROS scavenging capacity. Moreover, these results show that the 200°C powder does not play a key role in the scavenging capacity of ROS species, even at higher concentrations.

3.2.6 Evaluation of the presence of ROS inside the cells

Similar to the previous result, the intracellular ROS were analysed after 48h of culture with TiO_2 powders (Figure 3.8).

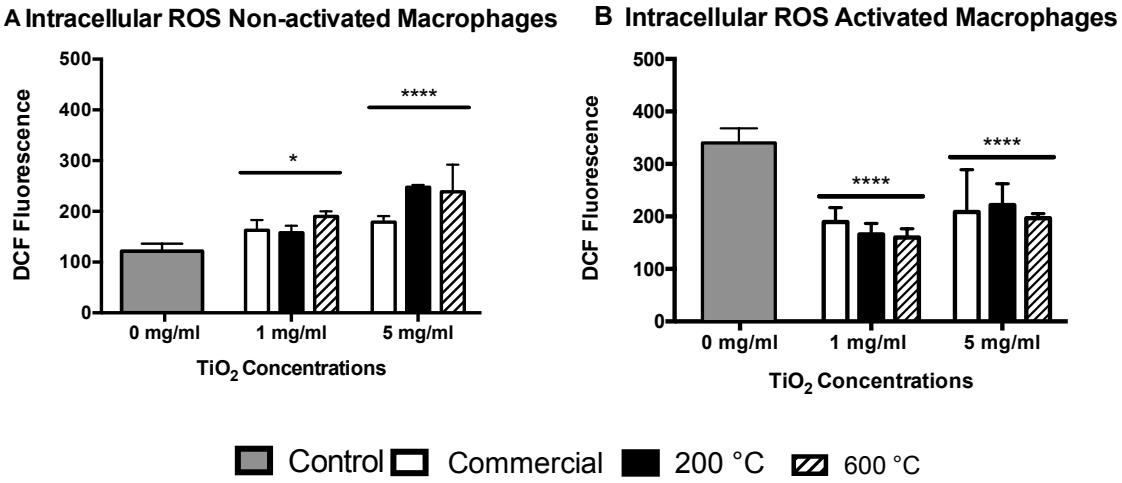

Figure 3.8 – DCF fluorescence after 48h of culture in the presence of powders, (quantified by flow cytometry after the macrophages were 1,5 hrs in contact with $DCFDAH_2$) proportional to the intracellular ROS. A – Extracellular ROS of the non-activated macrophages. B – Extracellular ROS of the activated macrophages. Data represents the mean ± S.D, (n=3-4), **** p <0,0001 within the non-activated or activated macrophages in the presence of 1 mg/ml and 5 mg/ml of the TiO_2 powders compared to the cells without powders. These statistic differences are determined by 2way ANOVA test.

When non-activated macrophages were in the presence of different TiO_2 powders at different concentrations (Figure 3.8A), it was possible to observe fluorescence, proportional to the ROS levels, which increases with more significance in the presence of 5 mg/ml of TiO_2 powders comparatively to the transwell system in the absence of TiO_2 powders. Under illumination with light, TiO_2 causes severe oxidative damage to cells (75), which leads to the generation of ROS. Nevertheless, this increase is not comparable to the observed upon macrophage activation with LPS.

Under an inflammatory profile and in the absence of powders, the macrophages produce higher levels of ROS as showed by the higher values of fluorescence in Figure 3.8B. Importantly, the fluorescence when these macrophages are in the presence of the powders is significantly reduced, which reflects a reduction of the ROS levels. Within the same concentration of TiO_2 powder and comparing different types of TiO_2 powders there is no significant difference in the fluorescence values. Additionally, a similar result is obtained when compared the two different concentrations of TiO_2 powders.

The ROS released by macrophages are scavenged for the TiO_2 powders, therefore it is hypothesized that they lead to the reduction of the oxidant stress in macrophages and consequently TiO_2 powders could halt the ROS overproduction by the cells.

3.3 Bioreactor

3.3.1 Evaluation of the permeability of the system with methylene blue

The permeability is an important and essential characteristic of the bioreactor system. This feature was the first one to be assessed (Figure 3.9), using methylene blue. Since it is a blue dye and the diffusion profile is easily observed due to the colour change in the bottom chamber. The methylene blue solution was in the upper chamber and water in the bottom one. A polycarbonate membrane divided both chambers.

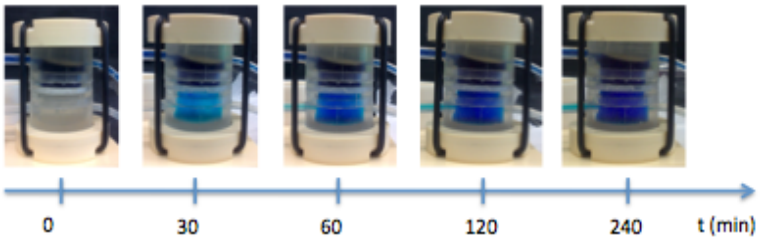

Figure 3.9 – Methylene blue diffusion from the upper to the bottom chamber through the polycarbonate membrne

This characteristic was tested under static conditions and dynamic conditions (Figure 3.10).

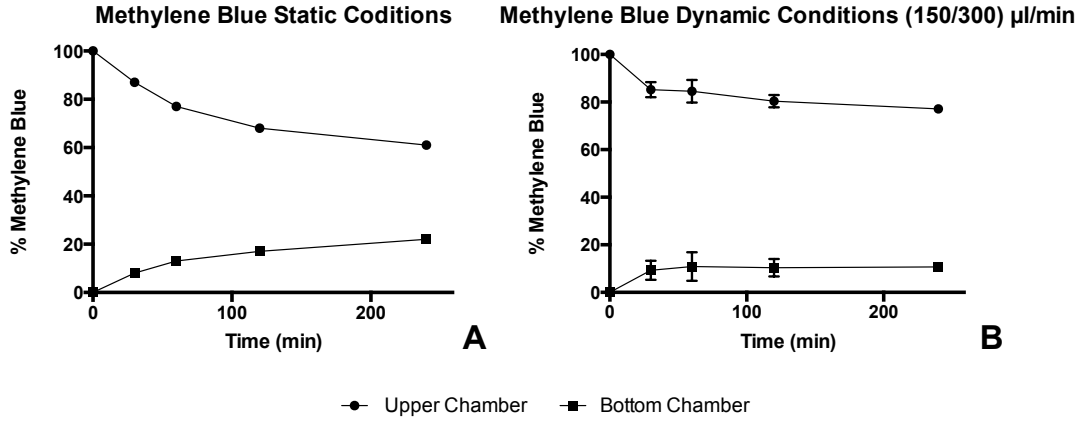

Figure 3.10 – Graphic representation of the methylene blue diffusion from the upper to the bottom chamber. A – Methylene blue diffusion under static conditions. B – Methylene blue diffusion under dynamic conditions with a flow rate of 150 µl/min and 300 µl/min for the bottom and upper chamber, respectively. Data represents the mean ± S.D, (n=3).

The diffusion of methylene blue, under static conditions, is gradual during the first hour and afterwards it is achieved a plateau region, when approximately 20 % of the methylene blue solution riches the bottom chamber. Under dynamic conditions the stabilization of the diffusion is achieved earlier, after 30 min. This stabilization is achieved after 10% of methylene blue passes through the membrane. It was expected that the decrease of methylene blue in the upper chamber was similar to the increase in the bottom chamber. However, according to the results obtained that is not the case, because we observe that a 50% equilibrium in not reached in both conditions. Therefore, the polycarbonate membrane acts as a barrier system where the methylene blue tends to deposit on the apical side of the membrane without translocation to the basal side. This effect, what was already observed in (76) is more representative under static conditions.

3.3.2 Evaluation of the ROS passage through the polycarbonate membrane – DPPH and SIN-1

The next step was to evaluate the passage of ROS molecules through the membrane from the upper to the bottom chamber. Firstly, the assay was performed with DPPH (Figure 3.11).

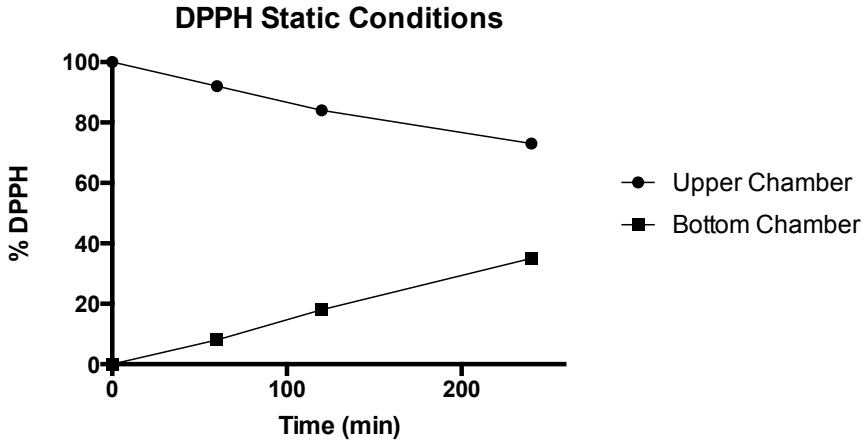

Figure 3.11 – Graphic representation of the DPPH diffusion from the upper to the bottom chamber under static conditions.

The diffusion of DPPH through the membrane under static conditions is linear during the 4h of the assay. It was not observed a stabilization of the diffusion similar to what occurs in the methylene blue assay. It was observed a diffusion approximately of 35 % of DPPH from the upper to the bottom chamber. The decay of the percentage in DPPH recorded in the upper chamber is similar to the increase in the bottom chamber. Nevertheless at the time point of 4h the solution from the upper chamber evaporates creating bubbles. Consequently the concentration of the solutions was altered and also the pressure system was not maintained. In this regard this assay was not performed under dynamic conditions and was tested other artificial ROS like SIN-1 (Figure 3.12).

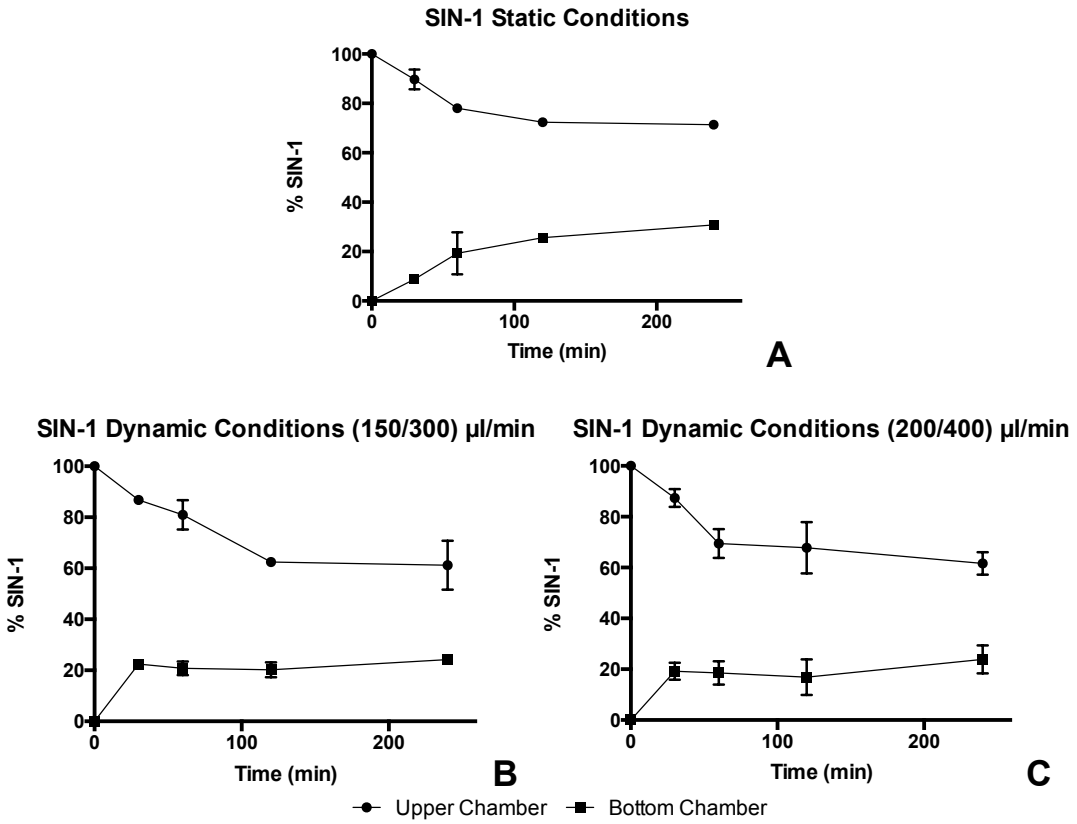

Figure 12 – Graphic represents the SIN-1 diffusion from the upper to the bottom chamber. A – SIN-1 diffusion under static conditions. B – SIN-1 diffusion under dynamic conditions with a flow rate of 150 µl/min and 300 µl/min for the bottom and upper chamber, respectively. C – SIN-1 diffusion under dynamic conditions with a flow rate of 200 µl/min and 400 µl/min for the bottom and upper chamber, respectively. Data represents the mean ± S.D, (n=2-4).

Identically to the methylene blue results, the diffusion of SIN-1 through the membrane occurs gradually and a steady state is finally achieved. The gradual diffusion of SIN-1 under static condition (Figure 12A) occurs for a period of 2h, while in dynamic conditions there is stabilization after 30 min. We can observe a decrease of about 40% of SIN-1 in the upper chamber. However, in the bottom chamber only 20% of SIN-1 was detected, which may indicate that some SIN-1 is being retained in the membrane, nonetheless contrasting to the methelyne blue results this effect is more significant under dynamic conditions. Moreover, it was tested if by increasing the flow rate was possible to modify the diffusion profile of SIN-1. As it is possible to observe on Figure 12B and C this increase did not change the diffusion profile through the membrane.

3.3.4 Culture of Macrophages in the bioreactor system

Once established the transwell model, we aiming to implement dynamic conditions and conduct similar assays with the previous ones. In this regard it was established at the same time a static system as control and a dynamic system with a flow rate of 150 µl/min for the bottom chamber and 300 µl/min upper chamber either with non-activated activated macrophages. The previous assays were performed after 48 hrs of incubation, therefore, in this assay was used the same time point.

Cell metabolic activity and evaluation the presence of ROS in the supernatant

Firstly, it was evaluated whether to implement dynamic conditions, the cell metabolic activity decreased (figure 3.13)

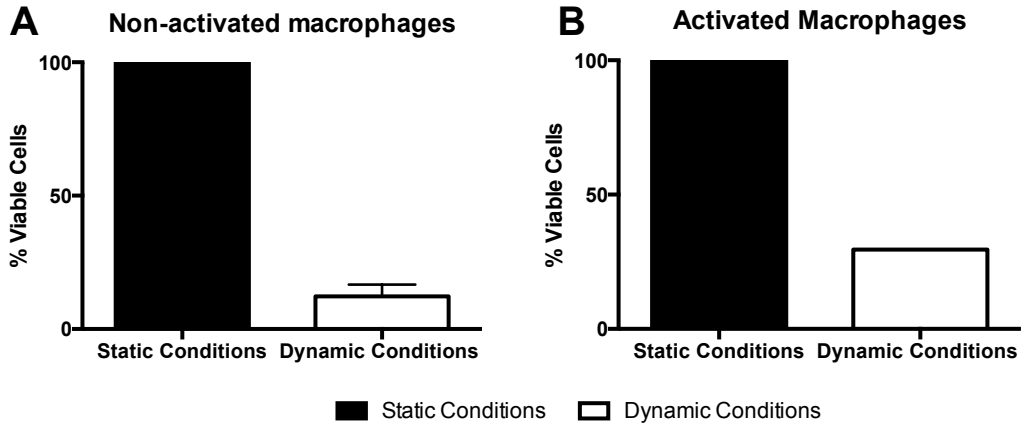

Figure 3.13 – Cell metabolic activity under static and dynamic conditions. A – Cell metabolic activity of non-activated macrophages. B – Cell metabolic activity of activated macrophages. Data represents the mean ± S.D, (n=1-2).

The cell metabolic activity from both non-activated and activated macrophages is significantly reduced when dynamic conditions were implemented. This reduction may have occurred due to the established flow rate. Firstly, in order to confirm the observed results we should make further replicas. Furthermore, other flow rates should be tested in order to find out if reducing the flow rate it is possible to increase the cell metabolic activity.

Despite the reduction in cell metabolic activity under dynamic conditions, it was, subsequently, analyzed the presence of ROS on both chambers (figure 3.14).

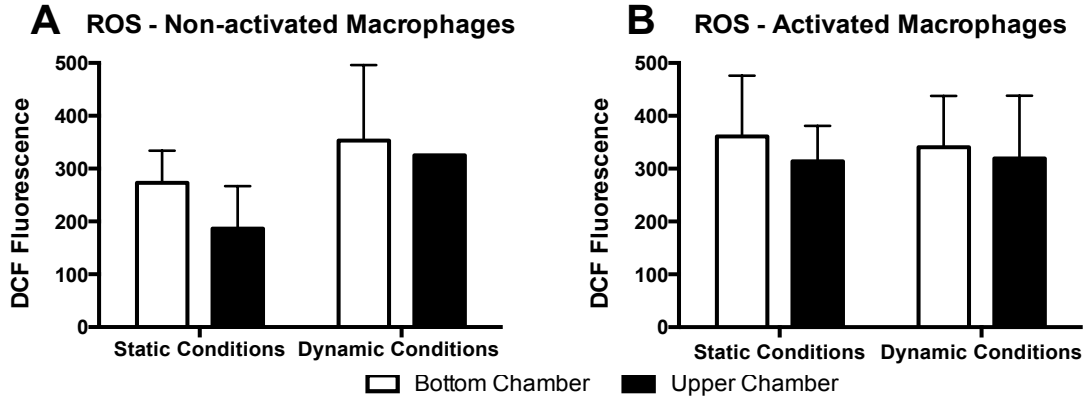

Figure 3.14 – DCF fluorescence, proportional to the extracellular ROS on the upper and bottom chamber under static and dynamic conditions. A – ROS of non-activated macrophages. B – ROS of activated macrophages. Data represents the mean ± S.D, (n=1-2).

In both non-activated and activated macrophages and also either under static or dynamic conditions the ROS levels in the bioreactor chambers is identically.

Whilst there is no significant difference between of static and dynamic conditions from the non-activated macrophages, there is an increment of fluorescence when non-activated macrophages were subjected to dynamic conditions, which may indicate that the flow rate applied could induce the cell activation. Nevertheless, due to the low cell viability under dynamic conditions, the respective ROS results should not be taking into account. To be certain of this result, more replicas should be performed. Moreover, other flow rates should be tested in order to evaluate in which one we can maintain the non-activated state.

Finally on this point, it was also addressed the incorporation of the TiO_2 powders on the system. Nevertheless, and knowing that the TiO_2 powder in the medium forms a suspension instead of a solution, the presence of loose TiO_2 powders in the system clogs the system and thereby preventing the normal flow rate and consequently the presence of a laminar flow. To circumvent this problem, we tried to incorporated the TiO2 powder into a hydrogel, but without success

Chapter 4

Conclusions and future perspectives

Conclusions and future perspectives

As more relevant conclusion remark, this work allows to conclude, either by chemical or biological tests, that TiO_2 powders presented a high ROS scavenging capacity, especially the 200°C and 600°C calcined powders.

Regarding the chemical assays, where the ROS scavenging capacity of different calcined TiO_2 powders (204757 commercial, 200°C, 600°C and 700°C) along with mixtures of different ratios of 200°C and 700°C TiO_2 powders were tested. Our findings indicated that the 200°C and 600°C presented the best ROS scavenging capacity. Moreover, the mixtures of the different powders did not improve the ROS scavenging capacity.

Once completed the chemical assays, it was used ROS produced by macrophages in order to understand if the ROS scavenging capacity of the most promising powders was maintained. In order to obtain a close-up view of what happens *in vivo* where the macrophages are not in direct contact with the TiO_2 particles, it was used a trans-well system (macrophages in the apical side and TiO_2 powders in the basal side). Two different concentrations of the 200°C and 600°C calcined TiO_2 powders were tested, 1 mg/ml and 5 mg/ml, and our findings indicted that, with both concentrations, the macrophages metabolic activity was maintained, and therefore, the powder had non-toxic properties at these concentrations. Regarding the ROS scavenging capacity, both powders as well as both concentrations revealed a similar profile. There was a significantly reduction of the ROS levels - both extracellular ROS and intracellular ROS - in the presence of the TiO_2 powders.

Finally, regarding the bioreactor system, it was evaluated the permeability of the used membrane by placing on the upper chamber a solution of methylene blue and, thereafter, artificial ROS. It was possible to observe a gradient of diffusion either of methylene blue or artificial ROS through the bioreactor membrane. Additionally, it was seen interactions between the analysed compounds and the polycarbonate membrane. Once this assay was concluded, some preliminary assays were performed with macrophages. The cells were seeded in the membrane and a flow rate – 300 µl/min for the upper chamber and 150 µl/min for the bottom chamber – was established. The results reveal a marked decrease in the cell viability when the

dynamic conditions were implemented. Concerning the ROS levels, they were similar for both conditions and also for the non-activated and activated macrophages. Nevertheless, a slightly increase in the ROS levels from the non-activated macrophages when established the dynamic conditions indicate a possible macrophage activation. However, as preliminary assays, it should be performed more replicas and tested different flow rates.

In conclusion, our results allow to consider that TiO_2 is a promising biomaterial regarding its ROS scavenging capacity, with a particular focus on the 200°C and 600°C calcined powders. Regarding the bioreactor system, the results allow us to conclude that this is a useful tool enabling the study of applied flow through a cell culture and further simulate the eye environment.

Future work concerning the transwell system with macrophages should include the analysis of anti- and pro-inflammatory cytokines such as IL-10 and TNF-α. Regarding the bioreactor system with the macrophages other flow rates should be tested and also the TiO_2 powders, which in this case should be incorporated in the PMMA substrate. Furthermore as future work to this project should include the introduction of more complexity to the model. Namely, by the use of endothelial and RPE cells both constituents of the oBRB. In this context, we could simulate oxidative stress into the cells that, consequently, leads to ROS production. In this way we could evaluate the effect of different TiO_2 powders at the BRB level. This model should firstly be implemented under static conditions and then, in order to mimic the *in vivo* environment of the eye, should be implemented in dynamic conditions.

References

1. Barar J, Asadi M, Mortazavi-Tabatabaei SA, Omidi Y. Ocular Drug Delivery; Impact of in vitro Cell Culture Models. J Ophthalmic Vis Res. 2009;4:239–52.

2. Cunha-Vaz JG. The blood-ocular barriers: past, present, and future. Doc Ophthalmol. 1997;93:149–57.

3. Chen MS, Hou PK, Tai TY, Lin BJ. Blood-ocular barriers. Tzu Chi Medical Journal. 2008. p. 25–34.

4. Kaur C, Foulds WS, Ling EA. Blood-retinal barrier in hypoxic ischaemic conditions: Basic concepts, clinical features and management. Progress in Retinal and Eye Research. 2008. p. 622–47.

5. Klaassen I, Van Noorden CJF, Schlingemann RO. Molecular basis of the inner blood-retinal barrier and its breakdown in diabetic macular edema and other pathological conditions. Progress in Retinal and Eye Research. 2013. p. 19–48.

6. Reichenbach A, Bringmann A. New functions of Müller cells. Glia [Internet]. 2013;61:651–78. Available from: http://www.ncbi.nlm.nih.gov/pubmed/23440929

7. Büssow H. The astrocytes in the retina and optic nerve head of mammals: a special glia for the ganglion cell axons. Cell Tissue Res. 1980;206:367–78.

8. Dorrell MI, Aguilar E, Jacobson R, Trauger SA, Friedlander J, Siuzdak G, et al. Maintaining retinal astrocytes normalizes revascularization and prevents vascular pathology associated with oxygen-induced retinopathy. Glia. 2010;58:43–54.

9. Gariano RF. Cellular mechanisms in retinal vascular development. Progress in Retinal and Eye Research. 2003. p. 295–306.

10. Bandopadhyay R, Orte C, Lawrenson JG, Reid AR, De Silva S, Allt G. Contractile proteins in pericytes at the blood-brain and blood-retinal barriers. J Neurocytol. 2001;30:35–44.

11. Hirschi KK, D'Amore PA. Pericytes in the microvasculature. Cardiovascular Research. 1996. p. 687–98.

12. Pautler EL, Tengerdy C. Transport of acidic amino acids by the bovine pigment epithelium. Exp Eye Res. 1986;43:207–14.

13. Boulton M, Dayhaw-Barker P. The role of the retinal pigment epithelium: topographical variation and ageing changes. Eye (Lond). 2001;15:384–9.

14. Simó R, Villarroel M, Corraliza L, Hernández C, Garcia-Ramírez M. The retinal pigment epithelium: something more than a constituent of the blood-retinal barrier--implications for the pathogenesis of diabetic retinopathy. J Biomed Biotechnol. 2010;2010:190724.

15. Booij JC, Baas DC, Beisekeeva J, Gorgels TGMF, Bergen AAB. The dynamic nature of Bruch's membrane. Progress in Retinal and Eye Research. 2010. p. 1–18.

16. Kawamura S, Tachibanaki S. Rod and cone photoreceptors: Molecular basis of the difference in their physiology. Comparative Biochemistry and Physiology - A Molecular and Integrative Physiology. 2008. p. 369–77.

17. Barar J, Asadi M, Mortazavi-Tabatabaei SA, Omidi Y. Ocular Drug Delivery; Impact of in vitro Cell Culture Models. J Ophthalmic Vis Res [Internet]. 2009;4:238–52. Available from: http://www.pubmedcentral.nih.gov/articlerender.fcgi?artid=3498862&tool=pmcentrez&rendertype=abstract

18. Zarbin MA. Current concepts in the pathogenesis of age-related macular degeneration. Arch Ophthalmol. 2004;122:598–614.

19. Ramrattan RS, van der Schaft TL, Mooy CM, de Bruijn WC, Mulder PG, de Jong PT. Morphometric analysis of Bruch's membrane, the choriocapillaris, and the choroid in aging. Invest Ophthalmol Vis Sci. 1994;35:2857–64.

20. Sparrow JR, Parish CA, Hashimoto M, Nakanishi K. A2E, a lipofuscin fluorophore, in human retinal pigmented epithelial cells in culture. Invest Ophthalmol Vis Sci. 1999;40:2988–95.

21. Wu Y, Fishkin NE, Pande A, Pande J, Sparrow JR. Novel lipofuscin bisretinoids prominent in human retina and in a model of recessive Stargardt disease. J Biol Chem. 2009;284:20155–66.

22. Espinosa-Heidmann DG, Suner IJ, Catanuto P, Hernandez EP, Marin-Castano ME, Cousins SW. Cigarette smoke-related oxidants and the development of sub-RPE deposits in an experimental animal model of dry AMD. Invest Ophthalmol Vis Sci. 2006;47:729–37.

23. De Jong PTVM. Age-related macular degeneration. N Engl J Med. 2006;355:1474–85.

24. Dardik R, Livnat T, Nisgav Y, Weinberger D. Enhancement of angiogenic potential of endothelial cells by contact with retinal pigment epithelial cells in a model simulating pathological conditions. Invest Ophthalmol Vis Sci. 2010;51:6188–95.

25. Kumar R, Harris-Hooker S, Kumar R, Sanford G. Correction: Co-culture of Retinal and Endothelial Cells Results in the Modulation of Genes Critical to Retinal Neovascularization. Vascular Cell. 2012. p. 6.

26. Hamilton RD, Foss AJ, Leach L. Establishment of a human in vitro model of the outer blood-retinal barrier. J Anat. 2007;211:707–16.

27. Capeáns C, Piñeiro A, Pardo M, Sueiro-López C, Blanco MJ, Domínguez F, et al. Amniotic membrane as support for human retinal pigment epithelium (RPE) cell growth. Acta Ophthalmol Scand. 2003;81:271–7.

28. Mamede AC, Carvalho MJ, Abrantes AM, Laranjo M, Maia CJ, Botelho MF. Amniotic membrane: from structure and functions to clinical applications. Cell and Tissue Research. 2012. p. 447–58.

29. Wisniewska-Kruk J, Hoeben KA, Vogels IMC, Gaillard PJ, Van Noorden CJF, Schlingemann RO, et al. A novel co-culture model of the blood-retinal barrier based on primary retinal endothelial cells, pericytes and astrocytes. Exp Eye Res. 2012;96:181–90.

30. Malina KCK, Cooper I, Teichberg VI. Closing the gap between the in-vivo and in-vitro blood-brain barrier tightness. Brain Res. 2009;1284:12–21.

31. Wang J, Xu X, Elliott MH, Zhu M, Le Y-Z. Müller cell-derived VEGF is essential for diabetes-induced retinal inflammation and vascular leakage. Diabetes. 2010;59:2297–305.

32. Park H-J, Zhang Y, Georgescu SP, Johnson KL, Kong D, Galper JB. Human umbilical vein endothelial cells and human dermal microvascular endothelial cells offer new insights into the relationship between lipid metabolism and angiogenesis. Stem Cell Rev. 2006;2:93–102.

33. Capetandes A, Gerritsen ME. Simplified methods for consistent and selective culture of bovine retinal endothelial cells and pericytes. Invest Ophthalmol Vis Sci. 1990;31:1738–44.

34. Mannermaa E, Reinisalo M, Ranta VP, Vellonen KS, Kokki H, Saarikko A, et al. Filter-cultured ARPE-19 cells as outer blood-retinal barrier model. Eur J Pharm Sci. 2010;40:289–96.

35. Vinci B, Murphy E, Iori E, Meduri F, Fattori S, Marescotti MC, et al. An in vitro model of glucose and lipid metabolism in a multicompartmental bioreactor. Biotechnol J [Internet]. 2012;7:117–26. Available from: http://www.ncbi.nlm.nih.gov/pubmed/21805642

36. Mazzei D, Guzzardi MA, Giusti S, Ahluwalia A. A low shear stress modular bioreactor for connected cell culture under high flow rates. Biotechnol Bioeng. 2010;106:127–37.

37. Vinci B, Murphy E, Iori E, Marescotti MC, Avogaro A, Ahluwalia A. Flow-regulated glucose and lipid metabolism in adipose tissue, endothelial cell and hepatocyte cultures in a modular bioreactor. Biotechnol J. 2010;5:618–26.

38. Vozzi F, Bianchi F, Ahluwalia A, Domenici C. Hydrostatic pressure and shear stress affect endothelin-1 and nitric oxide release by endothelial cells in bioreactors. Biotechnol J [Internet]. 2013; Available from: http://www.ncbi.nlm.nih.gov/pubmed/23959971

39. Tanaka Y, Yamato M, Okano T, Kitamori T, Sato K. Evaluation of effects of shear stress on hepatocytes by a microchip-based system. Measurement Science and Technology. 2006. p. 3167–70.

40. Vozzi F, Mazzei D, Vinci B, Vozzi G, Sbrana T, Ricotti L, et al. A flexible bioreactor system for constructing in vitro tissue and organ models. Biotechnol Bioeng. 2011;108:2129–40.

41. Mazzei D, Vozzi F, Cisternino A, Vozzi G, Ahluwalia A. A High-Throughput Bioreactor System for Simulating Physiological Environments. IEEE Trans Ind Electron. 2008;55.

42. Vinci B, Duret C, Klieber S, Gerbal-Chaloin S, Sa-Cunha A, Laporte S, et al. Modular bioreactor for primary human hepatocyte culture: medium flow stimulates expression and activity of detoxification genes. Biotechnol J. 2011;6:554–64.

43. Luthert PJ. Pathogenesis of age-related macular degeneration. Diagnostic Histopathol. 2011;17:10–6.

44. Coleman HR, Chan C-C, Ferris FL, Chew EY. Age-related macular degeneration. Lancet. 2008;372:1835–45.

45. Ambati J, Fowler BJ. Mechanisms of age-related macular degeneration. Neuron. 2012. p. 26–39.

46. Kassoff A, Kassoff J, Buehler J, Eglow M, Kaufman F, Mehu M, et al. A randomized, placebo-controlled, clinical trial of high-dose supplementation with vitamins C and E, beta carotene, and zinc for age-related macular degeneration and vision loss - AREDS Report No. 8. Arch Ophthalmol. 515 N STATE ST, CHICAGO, IL 60610 USA: AMER MEDICAL ASSOC; 2001;119(10):1417–36.

47. Bressler NM, Bressler SB, Congdon NG, Ferris FL, Friedman DS, Klein R, et al. Potential public health impact of Age-Related Eye Disease Study results: AREDS report no. 11. Arch Ophthalmol. 2003;121:1621–4.

48. Group MPS. Argon laser photocoagulation for neovascular maculopathy. Five-year results from randomized clinical trials. Arch Ophthalmol. 1991;109:1109–14.

49. Bressler NM. Photodynamic therapy of subfoveal choroidal neovascularization in age-related macular degeneration with verteporfin: two-year results of 2 randomized clinical trials-tap report 2. Archives of ophthalmology. 2001 p. 198–207.

50. VEGF Inhibition Study in Ocular Neovascularization (V.I.S.I.O.N.) Clinical Trial Group, Chakravarthy U, Adamis AP, Cunningham ET, Goldbaum M, Guyer DR, et al. Year 2 efficacy results of 2 randomized controlled clinical trials of pegaptanib for neovascular age-related macular degeneration. Ophthalmology [Internet]. 2006;113:1508.e1–1508.25. Available from: http://www.ncbi.nlm.nih.gov/pubmed/16828500

51. Rosenfeld PJ, Brown DM, Heier JS, Boyer DS, Kaiser PK, Chung CY, et al. Ranibizumab for neovascular age-related macular degeneration. The New England journal of medicine. 2006 p. 1419–31.

52. Curcio CA, Medeiros NE, Millican CL. Photoreceptor loss in age-related macular degeneration. Invest Ophthalmol Vis Sci. 1996;37:1236–49.

53. Khandhadia S, Cipriani V, Yates JRW, Lotery AJ. Age-related macular degeneration and the complement system. Immunobiology. 2012. p. 127–46.

54. Jarrett SG, Boulton ME. Consequences of oxidative stress in age-related macular degeneration. Molecular Aspects of Medicine. 2012. p. 399–417.

55. Beatty S, Koh H-H, Phil M, Henson D, Boulton M. The Role of Oxidative Stress in the Pathogenesis of Age-Related Macular Degeneration. Survey of Ophthalmology. 2000. p. 115–34.

56. Fletcher EC, Chong N V. Looking beyond Lucentis on the management of macular degeneration. Eye (Lond). 2008;22:742–50.

57. Yang D, Elner SG, Bian ZM, Till GO, Petty HR, Elner VM. Pro-inflammatory cytokines increase reactive oxygen species through mitochondria and NADPH oxidase in cultured RPE cells. Exp Eye Res. 2007;85:462–72.

58. Cannizzo ES, Clement CC, Sahu R, Follo C, Santambrogio L. Oxidative stress, inflamm-aging and immunosenescence. Journal of Proteomics. 2011. p. 2313–23.

59. Kauppinen A, Niskanen H, Suuronen T, Kinnunen K, Salminen A, Kaarniranta K. Oxidative stress activates NLRP3 inflammasomes in ARPE-19 cells-Implications for age-related macular degeneration (AMD). Immunol Lett. 2012;147:29–33.

60. Donoso LA, Kim D, Frost A, Callahan A, Hageman G. The role of inflammation in the pathogenesis of age-related macular degeneration. Survey of Ophthalmology. 2006. p. 137–52.

61. Ambati J, Atkinson JP, Gelfand BD. Immunology of age-related macular degeneration. Nat Rev Immunol [Internet]. 2013;13:438–51. Available from: http://www.ncbi.nlm.nih.gov/pubmed/23702979

62. Skeie JM, Mullins RF. Macrophages in neovascular age-related macular degeneration: friends or foes? Eye (Lond). 2009;23:747–55.

63. Ratner BD. A prespective on Titanium Biocompatibility. Titanium in Medicine: Material Science, Surface Science, Engineering, Biomedical Responses and Medical Application. 2001. p. 2–12.

64. Konaka R, Kasahara E, Dunlap WC, Yamamoto Y, Chien KC, Inoue M. Ultraviolet irradiation of titanium dioxide in aqueous dispersion generates singlet oxygen. Redox Rep. 2001;6:319–25.

65. Suzuki R, Muyco J, McKittrick J, Frangos JA. Reactive oxygen species inhibited by titanium oxide coatings. J Biomed Mater Res A. 2003;66:396–402.

66. Contreras R, Sahlin H, Frangos JA. Titanate biomaterials with enhanced antiinflammatory properties. J Biomed Mater Res - Part A. 2007;80:480–5.

67. Hanaor DAH, Sorrell CC. Review of the anatase to rutile phase transformation. Journal of Materials Science. 2011. p. 855–74.

68. Xiong S, Tang Y, Ng HS, Zhao X, Jiang Z, Chen Z, et al. Specific surface area of titanium dioxide (TiO2) particles influences cyto- and photo-toxicity. Toxicology. 2013;304:132–40.

69. Chen YF, Lee CY, Yeng MY, Chiu HT. The effect of calcination temperature on the crystallinity of TiO2 nanopowders. J Cryst Growth. 2003;247:363–70.

70. Zachariah A, Baiju K V., Shukla S, Deepa KS, James J, Warner KGK. Synergistic effect in photocatalysis as observed for mixed-phase nanocrystalline titania processed via sol-gel solvent mixing and calcination. J Phys Chem C. 2008;112:11345–56.

71. Zhang Y, Choksi S, Chen K, Pobezinskaya Y, Linnoila I, Liu Z-G. ROS play a critical role in the differentiation of alternatively activated macrophages and the occurrence of tumor-associated macrophages. Cell Res [Internet]. 2013;23:898–914. Available from: http://www.pubmedcentral.nih.gov/articlerender.fcgi?artid=3698641&tool=pmcentrez&rendertype=abstract

72. Covarrubias A, Byles V, Horng T. ROS sets the stage for macrophage differentiation. Cell Res [Internet]. 2013;23:984–5. Available from: http://www.ncbi.nlm.nih.gov/pubmed/23835480

73. Musa KH, Abdullah A, Kuswandi B, Hidayat MA. A novel high throughput method based on the DPPH dry reagent array for determination of antioxidant activity. Food Chem. 2013;141:4102–6.

74. Laguerre M, Hugouvieux V, Cavusoglu N, Aubert F, Lafuma A, Fulcrand H, et al. Probing the micellar solubilisation and inter-micellar exchange of polyphenols using the DPPH free radical. Food Chem. 2014;149:114–20.

75. Singh RJ, Hogg N, Joseph J, Konorev E, Kalyanaraman B. The peroxynitrite generator, SIN-1, becomes a nitric oxide donor in the presence of electron acceptors. Arch Biochem Biophys. 1999;361:331–9.

76. Tsuchiya S, Yamabe M, Yamaguchi Y, Kobayashi Y, Konno T, Tada K. Establishment and characterization of a human acute monocytic leukemia cell line (THP-1). Int J Cancer. 1980;26:171–6.

77. Qin Z. The use of THP-1 cells as a model for mimicking the function and regulation of monocytes and macrophages in the vasculature. Atherosclerosis. 2012. p. 2–11.

78. Dieter P, Schwende H. Protein kinase C-?? and -?? play antagonistic roles in the differentiation process of THP-1 cells. Cell Signal. 2000;12:297–302.

79. Fujihara M, Muroi M, Tanamoto KI, Suzuki T, Azuma H, Ikeda H. Molecular mechanisms of macrophage activation and deactivation by lipopolysaccharide: Roles of the receptor complex. Pharmacology and Therapeutics. 2003. p. 171–94.

80. Cai R, Kubota Y, Shuin T, Sakai H, Hashimoto K, Fujishima A. Induction of cytotoxicity by photoexcited TiO2 particles. Cancer Res. 1992;52:2346–8.

81. Giusti S, Sbrana T, La Marca M, Di Patria V, Martinucci V, Tirella A, et al. A novel dual-flow bioreactor simulates increased fluorescein permeability in epithelial tissue barriers. Biotechnol J. 2014;9:1–10.

Appendices

Appendix A

The following tables describe the supplier and the associated reference, for each material.

Chemical Assays

1. 2,2-diphenyl-1-picrylhydrazyl (DPPH) in the presence of titanium dioxide (TiO_2)

Material	Supplier / Reference
2,2-diphenyl-1-picrylhydrazyl (DPPH)	Sigma Aldrich® / D9132
Isopropanol	JMGS / 20904,362
Titanium dioxide (TiO_2)	Sigma Aldrich® / 204757
TiO_2 200°C	--
TiO_2 700°C	--

2. 3-Morpholinosyndnomine (SIN-1) in the presence of titanium dioxide (TiO_2)

Material	Supplier / Reference
3-Morpholinosyndnomine (SIN-1)	Sigma Aldrich® / M5793
2'-7'-dichlorodihydrofluorescein diacetate ($DCFDAH_2$)	Molecular Probes® (Invitrogen) / C-400
KOH	EMSURE® (Merck milipore) / 105033
Phosphate buffered saline (PBS)	
Sodium Chloride (NaCl)	EMSURE® (Merck milipore) / 106404
Potassium Chloride (KCl)	Sigma Aldrich® / P8041
Sodium phosphate dibasic (Na_2HPO_4)	EMSURE® (Merck milipore) / S106586
Monopotassium phosphate (KH_2PO_4)	Sigma Aldrich® / P5655
Artificial cerebrospinal fluid (aCSF)	
Sodium Chloride (NaCl)	EMSURE® (Merck milipore) / 106404
Calcium Chloride ($CaCl_2$)	EMSURE® (Merck milipore) / 102378
Potassium Chloride (KCl)	Sigma Aldrich® / 60133
D-Glucose	Fisher Chemical / G/0500/60
Magnesium chloride ($MgCl_2$)	EMSURE® (Merck milipore) / 105833
Phosphate buffered saline (PBS)	
Titanium dioxide (TiO_2)	Sigma Aldrich® / 204757
TiO_2 200°C	--
TiO_2 700°C	--

Cell Culture

1. Human monocytic leukemia cell line (THP-1) propagation, cell differentiation into macrophages and activation

Material	Supplier / Reference
RPMI 1640 GlutaMax	Gibco® (Life Technologies) / 61870-010

Fetal Bovine Serum (FBS)	Sigma Aldrich® / F7524
Penicillin / Streptomycin	Gibco® (Invitrogen)/ 15140-122
Trypsin	Sigma Aldrich® / T0646
Phorbol 12-myristate 13-acetate (PMA)	Sigma Aldrich® / P8139
Bacterial lipopolysaccharide (LPS)	Sigma Aldrich® / L6529

2. Transwell Assays: evaluate the viability, presence of ROS in the supernatant and inside the cell

Material	**Supplier / Reference**
Transwell inserts	VWR (Corning®) / 29442-086
RPMI 1640 GlutaMax	Gibco® (Life Technologies) / 61870-010
Fetal Bovine Serum (FBS)	Sigma Aldrich® / F7524
Penicillin / Streptomycin	Gibco® (Invitrogen)/ 15140-122
Phosphate buffered saline (PBS)	
Sodium Chloride (NaCl)	EMSURE® (Merck milipore) / 106404
Potassium Chloride (KCl)	Sigma Aldrich® / P8041
Sodium phosphate dibasic (Na_2HPO_4)	EMSURE® (Merck milipore) / S106586
Monopotassium phosphate (KH_2PO_4)	Sigma Aldrich® / P5655
Titanium dioxide (TiO_2)	Sigma Aldrich® / 204757
2'-7'-dichlorodihydrofluorescein diacetate ($DCFDAH_2$)	Molecular Probes® (Invitrogen) / C-400
Resazurin	Sigma Aldrich® / R7017
TiO_2 200°C	--
TiO_2 600°C	--

Bioreactor assays

Material	**Supplier / Reference**
Polycarbonate Membrane	Sigma Aldrich® / P9449-100EA
3-Morpholinosyndnomine (SIN-1)	Sigma / M5793
Artificial cerebrospinal fluid (aCSF)	
Sodium Chloride (NaCl)	EMSURE® (Merck milipore) / 106404
Calcium Chloride ($CaCl_2$)	EMSURE® (Merck milipore) / 102378
Potassium Chloride (KCl)	Sigma Aldrich® / 60133
D-Glucose	Fisher Chemical / G/0500/60
Magnesium chloride ($MgCl_2$)	EMSURE® (Merck milipore) / 105833
Phosphate buffered saline (PBS)	
Sodium Chloride (NaCl)	EMSURE® (Merck milipore) / 106404
Potassium Chloride (KCl)	Sigma Aldrich® / P8041
Sodium phosphate dibasic (Na_2HPO_4)	EMSURE® (Merck milipore) / S106586
Monopotassium phosphate (KH_2PO_4)	Sigma Aldrich® / P5655
2,2-diphenyl-1-picrylhydrazyl (DPPH)	Sigma Aldrich® / D9132
Isopropanol	JMGS / 20904,362